## NOTICE

The quality of this microform is heavily dependent upon the quality of the original thesis submitted for microfilming. Every effort has been made to ensure the highest quality of reproduction possible.

If pages are missing, contact the university which granted the degree.

Some pages may have indistinct print especially if the original pages were typed with a poor typewriter ribbon or if the university sent us an inferior photocopy.

Reproduction in full or in part of this microform is governed by the Canadian Copyright Act, R.S.C. 1970, c. C-30, and subsequent amendments.

## AVIS

La qualité de cette microforme dépend grandement de la qualité de la thèse soumise au microfilmage. Nous avons tout fait pour assurer une qualité supérieure de reproduction.

S'il manque des pages, veuillez communiquer avec l'université qui a conféré le grade.

La qualité d'impression de certaines pages peut laisser à désirer, surtout si les pages originales ont été dactylographiées à l'aide d'un ruban usé ou si l'université nous a fait parvenir une photocopie de qualité inférieure.

La reproduction, même partielle, de cette microforme est soumise à la Loi canadienne sur le droit d'auteur, SRC 1970, c. C-30, et ses amendements subséquents.

# A Mean Field Method for Disordered Magnetic Alloys with Application to FCC Fe-Ni

by

Paula R.L. Heron

Thesis Submitted to

the School of Graduate Studies and Research

in partial fulfilment of the requirements for the degree

of Master of Science in Physics

Physics Department

Faculty of Science

University of Ottawa

Ottawa, Canada

ISBN 0-315-75035-9

UNIVERSITÉ D'OTTAWA
UNIVERSITY OF OTTAWA

# ACKNOWLEDGEMENTS

I would like to thank Dr. Denis Rancourt for his guidance in this project. It has been a privilege to work under his supervision.

I would like to acknowledge the financial support provided by Dr. Rancourt, the University of Ottawa and NSERC.

I would like to thank Joanne and David Polsky, Lorraine Gravelle, Gilberte Lavoie and my family for the technical and/or moral support and Michel Bruyère for providing an incentive to finish this project.

Most of all I would like to thank my father for his company, his support and, last but not least, all the photocopying. In the end, it was sort of fun.

# ABSTRACT

We present a mean field model for the magnetism of random alloys. The reader is introduced to the philosophy of the mean field approach with an example of a simple ferromagnet. The special problem presented by random arrangement of alloy components on a lattice is discussed before we describe the technique we have developed. Our approach simplifies the treatment of these complicated systems by classifying sites according to the characteristics of their local environments. We apply this technique to both a fictional 1-D chain and to a real 3-D alloy series (fcc Fe-Ni). Fair success in modelling the complex magnetic behaviour characteristic of mixed exchange alloys (such as flattened magnetization curves, departure of the saturation moment from the Slater-Pauling curve, a complex phase diagram, and para-process susceptibility) is achieved.

# CONTENTS

# LIST OF FIGURES

# 1/ INTRODUCTION

Random magnetic binary alloys are the subject of the research project presented herein. Such systems do not as yet lend themselves to analytic investigation because of their complexity and therefore we have sought some approximate method of modelling their magnetic behaviour. The approach we have developed belongs to the class of techniques known as *effective* or *mean field theories* (MFT). In contrast to mean field theories of simple ferromagnets (where all atoms are identical and occupy crystallographically equivalent lattice sites), or antiferromagnets and ferrimagnets (where the lattice may be divided into a few sets of equivalent sites or *sublattices*), our method deals with a system in which no two sites are the same.

We have developed a technique which is (1) simple in both concept and execution and (2) delivers most features of a real system. The assumptions we have made are described in Section 7.1. Our model is general and adheres closely to the mean field theory while employing one new physical approximation, introduced in Section 1.2 and presented in detail in Chapter 4.

## 1.1 THE CHALLENGE

The test of our model was performed with real data on the Fe-Ni alloys, systems which have been well studied but are as yet not fully understood. These alloys, because they contain both ferro- and antiferromagnetic interactions and have itinerant electrons, challenge simple techniques.

We have calculated the following quantities, all of which have characteristic features for such alloys. The temperature dependence of magnetization is flattened with respect to that seen in pure ferromagnets, transition temperatures have a characteristic composition dependence, saturation moments deviate from the Slater-Pauling curve, high field susceptibilities indicate failure of the system to saturate under conditions which saturate ferromagnets, and hyperfine field distributions are broad implying magnetic inhomogeneity.

## 1.2 THE NOVEL STRATEGY

The problem with random alloys is that there are $N$ ($\sim 10^{23}$) distinguishable lattice sites which we will label with $i$. If we consider a local property $F_i$ which depends on the environment of the site, then, in order to average over all sites, we would have to know the value of that property for each site $\{F_1,F_2,\ldots F_i,\ldots\}$. As there is no general expression for the quantities we wish to consider (thermally averaged local moments, hyperfine fields...) and we cannot consider each site individually, we introduce an approximation. We classify each site according to the species residing there and its local environment and replace the real distribution over $N$ sites to one over $C$ *classes*.

Then we can replace:

$$\overline{F}^{true} = \frac{1}{N}\sum_{i=1}^{N} F_i \qquad (1)$$

with an approximation:

$$\overline{F}^{appr.} = \sum_{k=1}^{C} P(k)\, F_k. \qquad (2)$$

where $k$ labels the classes. We would expect to find that:

$$\lim_{C\to N} \overline{F}^{appr.} \to \overline{F}^{true}. \qquad (3)$$

Our model starts by distinguishing the two different species in a binary alloy (*Zeroth Order Class*) and for each, defines the local environment to include only the species identity of the *first* nearest neighbours. This is the *First Order Model*. Summing over the First Order Classes then leads to the species average for a property; summing over the species averages leads to the system average. We successively refine the approach by considering further coordination shells in our classification scheme, (*Second* and *Third Order Classes* etc.). Results for the 1-D linear chain alloy display the convergence predicted by Eq.(3) as higher order classes are considered.

As a point of comparison we include the *Average Interaction* and *Average Environment* models. Such models assign the same effective qualities to each atom in the system, the opposite of the actual situation. Our models provide a compromise between the two extreme viewpoints: one in which each site must be explicitly considered (excessively difficult in execution) and the other in which all sites are considered to be the same (excessively simple in concept). Each model in our hierarchy provides a different payoff in terms of the quality of results versus the level of practical difficulty; a choice to be made by the end user.

## 1.3 ESSENTIAL BACKGROUND

Familiarity with basic quantum mechanics and statistical mechanics is assumed as well as some knowledge of topics such as paramagnetism, exchange interactions, the spin Hamiltonian and ferromagnetism, all subjects covered in standard textbooks such as Solid State Physics by Ashcroft and Mermin [1]. A list of symbols and abbreviations used is appended.

## 1.4 OVERVIEW OF THE THESIS

In Chapter 2 we present an example of mean field theory as applied to a ferromagnetic pure substance[1]. In Section 2.4 we discuss the application of mean field theory to ferrimagnets, in order to introduce the mathematics required when more than one species is present.

Chapter 3 presents the Average Interaction and Average Environment Models as examples of overly simple MFT approaches to random alloys.

---

[1] Effective Field Theories of Magnetism by J.S. Smart [2] provides an excellent review of the subject of MFT as applied to pure substances and compounds.

We present our method, referred to as *Classification by Near Neighbour Environments*, in detail for the First Order Model in Chapter 4. This Chapter illustrates the way in which MFT is adapted for use with an atomically random system. The application of Second and Third Order models to a 1-D alloy is the subject of Chapter 5.

In Chapter 6 a specific case of ferrimagnet is examined, in order to isolate the effects of randomness from those of multiple spin types and exchange constants. We demonstrate that flattened magnetization curves can arise from randomness without requiring mixed exchange. Mixed exchange refers to that situation in which some spin-spin interactions favour parallel alignment while others favour anti-parallel alignment.

Chapter 7 outlines the generalization of our model for systems which contain itinerant electrons, imperfect randomness, and mixed exchange. The implications of mixed exchange for both real systems and a simple model are discussed. The procedure for modelling the properties of a real system is presented in Section 7.6.

The test of our model against a real system with some of the above features is the subject of Chapter 8. Sections 8.2 through 8.5 describe the calculation of the macroscopic and microscopic features which we are interested in and able to calculate, and the degree of agreement with experiment attained.

Note that we do not include magneto-elastic coupling in our model or even consider the phonon degrees of freedom such that "Invar behaviour" itself is not modelled or explained in this thesis.

# 2/ MEAN FIELD THEORY - GENERAL INFORMATION

## 2.1 PHILOSOPHY

### 2.1.1 Spin-Spin Interactions

The *exchange* interaction between magnetic moments[2] is of quantum mechanical origin and makes spin alignment (↑ ↑ or ↑ ↓) energetically favourable. The Hamiltonian of the $i^{th}$ ion is:

$$H_i = \sum_{j \neq i}^{N-1} -J_{ij} \vec{S}^i \cdot \vec{S}^j \qquad (4)$$

where $J_{ij}$ is the *exchange constant* for the bond between spins $i$ and $j$ and $\vec{S}^i$ is the spin angular momentum operator for the $i^{th}$ ion. The index $j$ runs over the spins of the system. Often, only terms including near neighbour pairs are significant and for the purposes of this project we have limited the range of the exchange interaction to the $z$ nearest neighbours only. (However, our model may be easily adapted if bonds between next or third nearest neighbours etc. must be included, as described in Section 7.5.)

---

[2] The magnetic moment is proportional to spin, we use these terms interchangeably: $\vec{\mu} = g\mu_B \vec{S}$.

### 2.1.2 The Mean Field Substitution

The basic premise of the mean field theory approach is that the problem may be recast in the mould of *paramagnetism* in which the spins do not interact with one another but with an applied field ($\vec{H}$). Each paramagnetic spin attempts to minimize its energy by aligning itself with the external field with a degree of success determined by thermal disordering effects. As a result, the thermally averaged spin, zero in the absence of a field, has some finite value. In exchange driven systems it is the interaction between neighbouring spins which leads to mutual alignment even in the absence of an external field.

Mean field theory asks the question *"What simple field, would, if applied to a spin through a paramagnetic interaction, give rise to that response which is seen in spontaneously magnetized systems; an average spin which, as the temperature rises, decreases at an increasingly rapid rate until vanishing altogether at a well-defined temperature?"* One answer, as we shall see, is a field proportional to the average spin itself. Thus we substitute a simple paramagnetic interaction for the complicated spin-spin one and our system becomes one of *N independent* ions. In a paramagnet, the external field is unaffected by an increase in temperature but it engenders a smaller response due to thermal effects. If the field itself is also decreasing, a second order phase transition is simulated.

The advantage of the substitution is clear: we need only consider a single-spin Hamiltonian, the solution of which is well known. Here we will illustrate the procedure for a Heisenberg ferromagnet. This example provides a framework which all MFT calculations follow.

### 2.1.3 The Zeeman Hamiltonian

The interaction of a paramagnetic ion with an applied field is governed by the Zeeman Hamiltonian:

$$H_Z^i = -g_i \mu_B \vec{S}^i \cdot \vec{H} \qquad (5)$$

where $\mu_B$ is the Bohr magneton, and $g$ is the Landé $g$-factor for the ion in the solid. Note that this Hamiltonian contains only the spin operator for the site in question. Orbital angular momentum is taken to be quenched [1].

## 2.2 THE SIMPLE FERROMAGNET

### 2.2.1 Description

The magnet may be of any dimension as this information appears only in the coordination number of the lattice. The lattice (1-D chain, 2-D square, 3-D cubic etc.) is perfect and occupied on each site by permanent magnetic moments. In a ferromagnet[3], minimization of the energy of the $i^{th}$ moment is achieved by its mutual parallel alignment with its neighbours.

Ferromagnets, in the presence of an applied field, have a Zeeman term in their spin Hamiltonian which fortifies the tendency toward spin alignment. At temperatures sufficiently high to confound the effects of exchange the effect of the Zeeman term dominates and the system is paramagnetic.

---

[3] It is important to distinguish between ferromagnetic *interactions* (J>0) and ferromagnetic *systems* in which such interactions lead to a finite spontaneous magnetization for $T<T_C$.

### 2.2.2 Macroscopic Features

The chief magnetic feature which we are interested in is the thermal average spin on the $i^{th}$ site given by:

$$\langle \vec{S}^i \rangle = \frac{Tr\, \vec{S}^i e^{-\beta H(\vec{S}^1, \vec{S}^2, \ldots \vec{S}^i, \ldots)}}{Z} \qquad (6)$$

$Z$

where $\beta = \frac{1}{k_B T}$ ; $k_B$ and $T$ being the Boltzmann constant and temperature respectively.

is known as the partition function and is defined as follows:

$$Z = Tr\, e^{-\beta H}. \qquad (7)$$

We can define a spatial/thermal average spin as follows:

$$\langle \vec{S} \rangle = \frac{1}{N} \sum_{i=1}^{N} \langle \vec{S}^i \rangle . \qquad (8)$$

A finite spatial/thermal average spin, arising *spontaneously* from the interactions between moments, and persisting at low temperatures is a measurable quantity and the hallmark of ferromagnets as shown in fig.1. Such a curve will also be referred to as the *magnetization curve*[4].

---

[4] magnetization = $\frac{Ng\mu_B \langle \vec{S} \rangle}{Vol.}$.

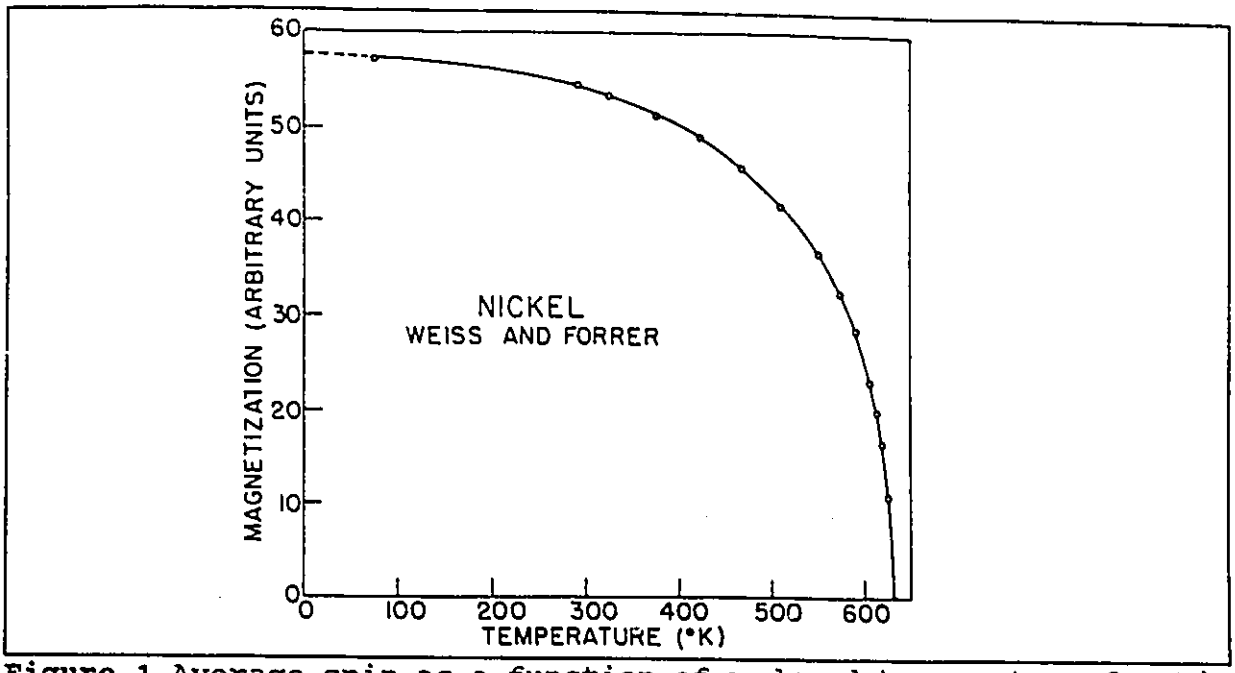


**Figure 1** Average spin as a function of reduced temperature for Ni. Smart [2], (after Weiss and Forrer, *Ann. Phys.* 5, 153 (1926).)

## 2.3 MFT SOLUTION OF THE SIMPLE FERROMAGNET

### 2.3.1 Strategy

We will see that by formulating a new Hamiltonian, calculations become accessible. We invoke mean field theory by replacing each spin in the first coordination shell of the $i^{th}$ spin by its thermal average. Eq.(5) becomes a mean field Hamiltonian:

$$H_m^i = -J\vec{S}^i \cdot \sum_{j=1}^{z} \langle \vec{S}^j \rangle . \qquad (9)$$

We note that in this system, in which all spins are indistinguishable on the basis of local environment, the thermal average on one spin is identical to that on every other[5] so that we may drop the index *i*.

[5] Neglecting edge effects etc., i.e. in the thermodynamic limit.

Using:

$$\langle \vec{S}^{\,i} \rangle = \langle \vec{S}^{\,j} \rangle \tag{10}$$

or:

$$\langle \vec{S} \rangle = \langle \vec{S} \rangle \tag{11}$$

we can write:

$$H_m = g\mu_B \vec{S} \cdot \lambda \langle \vec{S} \rangle \tag{12}$$

with:

$$\lambda = \frac{Jz}{g\mu_B}. \tag{13}$$

Note that this is exactly the form of the Zeeman Hamiltonian with $\lambda \langle \vec{S} \rangle$ playing the role of a mean or effective field. In this manner we have constructed a mean field from the thermal average spin of the exchange-linked neighbours of the central spin and effected the mean field substitution.

We have assumed that the mean field is identical throughout the magnet and now we take its direction to be the quantization axis for the spins so that:

$$H_m = -g\mu_B \vec{S} \cdot \overline{\mathrm{H}} = -g\mu_B S_z \overline{\mathrm{H}} \tag{14}$$

where $S_z$ is the z component of spin and $\overline{\mathrm{H}}$ is the mean field.

The mean field is then[6]:

$$\overline{H} = \lambda \langle S_z \rangle . \tag{15}$$

Note that $S_z$ is an operator while $\langle S_z \rangle$ is a dimensionless real number.

We may now calculate the thermal average for the z component of a spin using Eqs.(6) and (7) to get:

$$\langle S_z \rangle = \frac{Tr S_z e^{-\beta H(S_z)}}{Z} . \tag{16}$$

This problem is already solved [1]. Eq.(16) gives rise to the *Brillouin function*[7] which is represented symbolically by $B_S(x)$. Thus Eq.(16) becomes:

$$\langle S_z \rangle = S B_S(\beta J z S \langle S_z \rangle) , \tag{17}$$

the *mean field equation.*

### 2.3.2 Solving the Mean Field Equation

A solution for $\langle S_z \rangle$ may be found numerically. Graphically, the solution is represented by the intersection of the line $y = \langle S_z \rangle$ with the curve $y = SB_S(\beta J z S \langle S_z \rangle)$ as illustrated in fig.2 for several temperatures. Note that for $T < T_C$ there is an intersection, for $T = T_C$ the two functions are coincident near the origin and for $T > T_C$ there is no intersection.

---

[6] $\langle \vec{S} \rangle_z = \langle S_z \rangle \because \langle S_x \rangle = \langle S_y \rangle = 0$.

[7] $B_S(x) = \frac{2S+1}{2S} \coth\left(\frac{2S+1}{2S} x\right) - \frac{1}{2S} \coth\left(\frac{1}{2S} x\right)$.

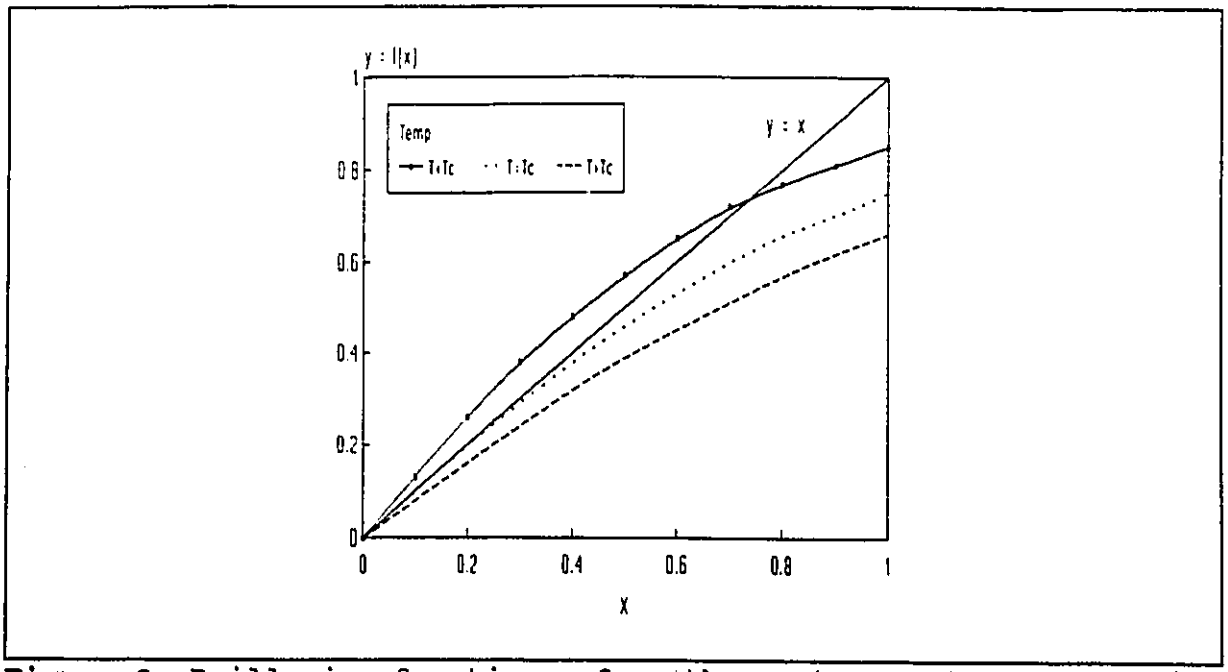


**Figure 2** Brillouin functions for three temperatures, showing solution of the mean field equation. *(S = 1, J = 40K).*

In this manner we can calculate the average spin at any temperature. We find that as the temperature increases the magnetization decreases at an accelerating rate, finally vanishing abruptly as shown for sample parameters in fig.3. Note the similarity to fig.1.

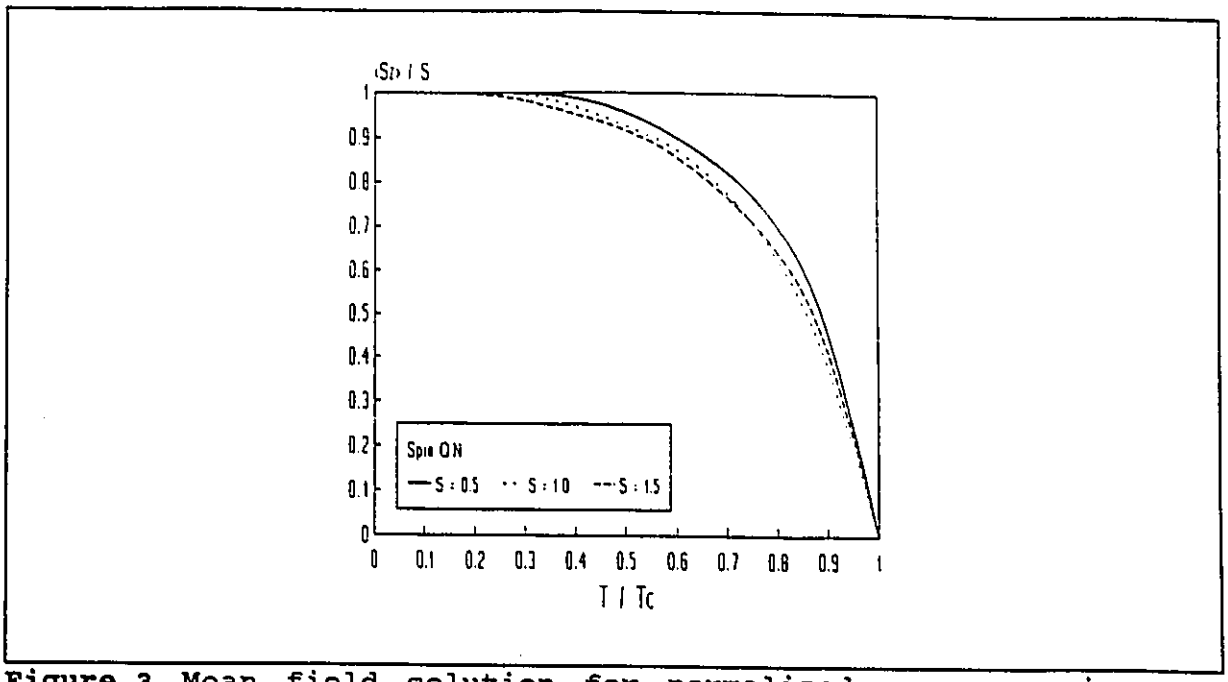


**Figure 3** Mean field solution for normalized average spin as a function of $T/T_C$ for different $S$'s. $T_C$ as in Eq.(20).

### 2.3.3 The Curie Temperature

In order to find the point of phase transition, known as the Curie temperature or $T_C$, we note that this is the temperature at which $<S_z>$ becomes non-zero on cooling in zero field. Just below $T_C$ the temperature is large while the average spin is small, making the entire argument of the Brillouin function small. We expand this function in a Taylor series [1] and, keeping terms up to first order, we find:

$$B_S(Sx) \approx \frac{(S+1)\,x}{3}, \qquad (18)$$

making Eq.(17) a *linear* function in $<S_z>$. The only condition under which this line will intersect *non-trivially* with $y = <S_z>$ is if the slope of Eq.(17) = 1.

This condition:

$$1 = \frac{S(S+1)}{3}\beta Jz, \tag{19}$$

determines the Curie temperature:

$$T_C = \frac{S(S+1)}{3k_B}Jz. \tag{20}$$

## 2.4 THE SIMPLE FERRIMAGNET

In contrast to the ferromagnet we investigated above, a ferrimagnet is *not* composed of a single species and all sites on the lattice are, therefore, *not* equivalent. In contrast to the *random* alloy however, the species are arranged so as to occupy interpenetrating *sublattices*.

The nearest neighbours of atoms on each sublattice are atoms on the *other* sublattice in the typical 2-D square lattice ferrimagnet shown in fig.4. If we follow the reasoning developed above we see that for atoms on sublattice *A* the mean field is dependent on the average spin of atoms on sublattice *B* and vice versa.

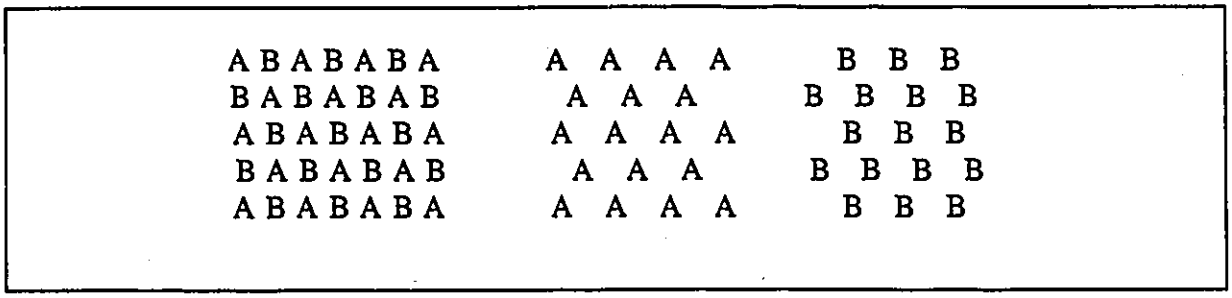


**Figure 4** Sublattices of a typical 2-D square lattice ferrimagnet.

The result is two simultaneous equations in two unknowns which may be solved numerically:

$$\begin{aligned} \langle S_z^A \rangle &= S^A B_{S^A}(\beta J_{AB} z S^A \langle S_z^B \rangle) \\ \langle S_z^B \rangle &= S^B B_{S^B}(\beta J_{AB} z S^B \langle S_z^A \rangle) \,. \end{aligned} \tag{21}$$

This development depends on the fact that for a given sublattice all sites are equivalent and hence the thermal average on a given site is equal that on every other. We shall see in the analysis of the random alloy that this identity does not apply; our new approximation is designed to account for this.

# 3/ OVERLY SIMPLE MFT METHODS FOR RANDOM ALLOYS

## 3.1 THE AVERAGE INTERACTION AND AVERAGE ENVIRONMENT MODELS

These models reduce the complexity of the random alloy by imagining a single mean field for every atom in the system or every atom of a particular species.

### 3.1.1 The Average Interaction Model

One method of dealing with the distribution of sites is to ignore it and assign each one the same qualities. One such attempt utilizes an *Average Interaction* (AI). Each atom is given an effective spin quantum number which is simply the geometric average of those of the two species:

$$S = c(A)\, S^A + c(B)\, S^B. \tag{22}$$

Then, to each pairwise interaction we assign an effective exchange constant $J$ for the average interaction calculated as follows:

$$J = P(AA)\, J_{AA} + P(AB)\, J_{AB} + P(BB)\, J_{BB} \tag{23}$$

where the probabilities for the three possible bonds are:

$$\begin{aligned} P(AA) &= c(A)^2 \\ P(AB) &= 2 \cdot c(A)\, c(B) \\ P(BB) &= c(B)^2 . \end{aligned} \tag{24}$$

Now we have reduced the problem to one identical to the ferromagnet of Chapter 2. The Curie point is found using $J$ and $S$ in Eq.(20). This process, though simple to apply, clearly denies the complex reality of the system and can be expected to mask many of the features of the alloys we are interested in. For instance, this model makes it impossible to calculate a distribution of hyperfine fields, known to occur in real alloys. We conclude that more detail must be allowed, even if it means a considerable increase in difficulty.

### 3.1.2 The Average Environment Model

Another overly simple approach assigns each spin of species *A* an *Average Environment* (AE) by summing over the possible nearest neighbour configurations. The mean field is constructed as follows:

$$\overline{H}_A = \sum_{n=0}^{z} P(z,n)\left(n\frac{J_{AA}}{g\mu_{B_B}}\langle S_z^A\rangle + (z-n)\frac{J_{AB}}{g\mu_B}\langle S_z^B\rangle\right). \qquad (25)$$

Where $P(z,n)$ is the probability (given in Eq.(27) below) for an *A*-type atom to have $n$ *A*-type nearest neighbours out of a possible $z$. The mean field for a *B*-type atom is constructed analogously. Thus we have two equations in two unknowns as in the case of the ferrimagnet. The coupled equations are:

$$\langle S^A\rangle = S^A B_{S^A}(\beta g\mu_B S^A \overline{H}_A) \qquad (26)$$
$$\langle S^B\rangle = S^B B_{S^B}(\beta g\mu_B S^B \overline{H}_B)$$

While this model is slightly more sophisticated than the average interaction model, it still precludes the calculation of microscopic qualities and the results for macroscopic qualities are expected to be of low quality given the degree of over-simplification.

# 4/ CLASSIFICATION BY NEAR NEIGHBOUR ENVIRONMENTS - OUR MODEL

As mentioned in Section 2.4, with a random alloy it is no longer possible to use the thermal average spin on different sites interchangeably. We note that the thermal averages constitute a continuous distribution and that in reality each spin feels a mean field of a different magnitude. In Section 1.2 we introduced our novel method of classifying sites according to their near neighbour environments thereby substituting a discrete distribution of fields and spin averages.

It is reasonable to assume that spins which have similar local environments will have similar mean fields and hence thermal averages, enough so that we can approximate that they are in fact the same. Our first step is to define local environment to mean the first coordination shell.

## 4.1 THE FIRST ORDER MODEL

We recall that the species of an atom is its Zeroth Order Class (ZOC). The First Order Class (FOC) of an atom depends on the ZOC of its nearest neighbours; hence the nomenclature: assignment of an ion to a First Order Class requires the identity of its *first* nearest neighbours.

We can define FOCs for a 1-D alloy as follows:

| | |
|---|---|
| A,0 | B A B |
| A,1 | B A A *or* A A B |
| A,2 | A A A |

**Figure 5** FOCs for an *A*-type atom.

### 4.1.1 Class probabilities

An alloy which is perfectly random at any concentration and temperature as well as being defect-free has a probability of finding an atom of one particular species on any given site given by the concentration *c(A)* alone, uncorrelated to the occupation of any other site. Therefore the probability of finding a particular nearest−neighbour configuration depends on the binomial formula. For instance, the probability of finding an atom of any type with $n$ $A$−type nearest neighbours among $z$ is given by:

$$P(z,n) = \frac{c(A)^n c(B)^{(z-n)} z!}{n!\ (z-n)!}. \qquad (27)$$

Note that $n$ will always be used to label the number of $A$-type nearest neighbours. The probability of finding an $A$-type atom with such a configuration is:

$$P(A,z,n) = P(A)\,P(z,n) = c(A)\,P(z,n). \qquad (28)$$

### 4.1.2 Constructing the Mean Field

We begin by considering an atom of FOC $A,n$ (an atom of type $A$ with $n$ $A-$type nearest neighbours). We cannot simply replace the $A$ and $B$-type neighbour spins with their thermal averages as this quantity is not defined. Instead we use the spatial/thermal averages defined below in Eq.(29). We construct the mean field as follows:

$$\overline{H}_{A,n} = n\frac{J_{AA}}{g\mu_B}\langle\overline{S}_z^A\rangle + (z-n)\frac{J_{AB}}{g\mu_B}\langle\overline{S}_z^B\rangle \qquad (29)$$

We have then $(z + 1)$ FOCs and mean fields for each species.

Most of the physics in a MFT model is contained in the construction of an appropriate mean field or set of mean fields. Once this has been achieved calculating the various properties more or less follows.

### 4.1.3 Average Spin Calculations

Given the mean field we can calculate the thermal average for this class of spin as in Eq.(6). In the spirit of Eq.(2) we can find the spatial/thermal average for the species, as follows:

$$\langle\overline{S}_z^A\rangle = \sum_{n=0}^{z} P(z,n)\,\langle S_z^{A,n}\rangle$$
$$\langle\overline{S}_z^B\rangle = \sum_{n=0}^{z} P(z,n)\,\langle S_z^{B,n}\rangle \qquad (30)$$

Now we have two equations in two unknowns which may be solved numerically to find the spin average for the ZOCs.

The equations are:

$$\langle \bar{S}_z^A \rangle = \sum_{n=0}^{z} P(z,n)\, S^A B_{S^A}\left( \frac{\beta}{g\mu_B} \left( nJ_{AA} \langle \bar{S}_z^A \rangle + (z-n) J_{AB} \langle \bar{S}_z^B \rangle \right) \right) \qquad (31)$$

$$\langle \bar{S}_z^B \rangle = \sum_{n=0}^{z} P(z,n)\, S^B B_{S^B}\left( \frac{\beta}{g\mu_B} \left( nJ_{AB} \langle \bar{S}_z^A \rangle + (z-n) J_{BB} \langle \bar{S}_z^B \rangle \right) \right).$$

With two quantities to solve for, the calculations are not much more complicated than in the AI model of Section 3.1.1, but we have acknowledged a higher level of detail.

Note that we have allowed the same amount of detail as the AE model of Section 3.2 but that Eqs.(31) are not the same as Eqs.(26). We have here a species average which is a sum over Brillouin functions, each of which involves a single, environment-specific mean field. In the AE model, on the other hand, the species average is a single Brillouin function for a mean field which is a sum over the possible environments. Thus the AE model averages "earlier" than does the FO model.

### 4.1.4 Results

The results of solving these two equations at a series of temperatures and for particular parameters are shown in fig.6a.

The results may be combined to get an overall average spin per atom as follows:

$$\langle \bar{S}_z \rangle = c(A) \langle \bar{S}_z^A \rangle + c(B) \langle \bar{S}_z^B \rangle . \qquad (32)$$

The average spin per atom vs. temperature curve is shown in fig.6b along with the result of the AI model for the same parameters.

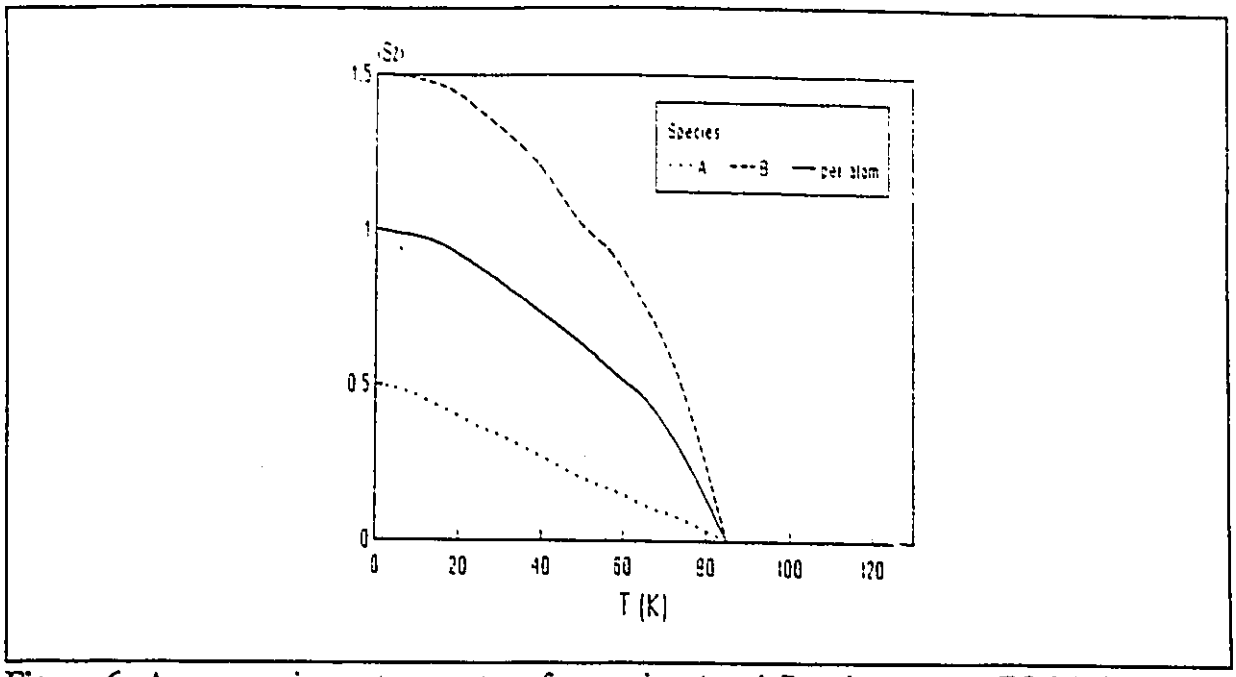


**Figure 6a** Average spin vs. temperature for species *A* and *B* and per atom. FO Model. $J_{AA}$ = 20K, $J_{AB}$ = 40K, $J_{BB}$ = 60K, $S^A$ = 0.5, $S^B$ = 1.5, c(A) = 50 at%.

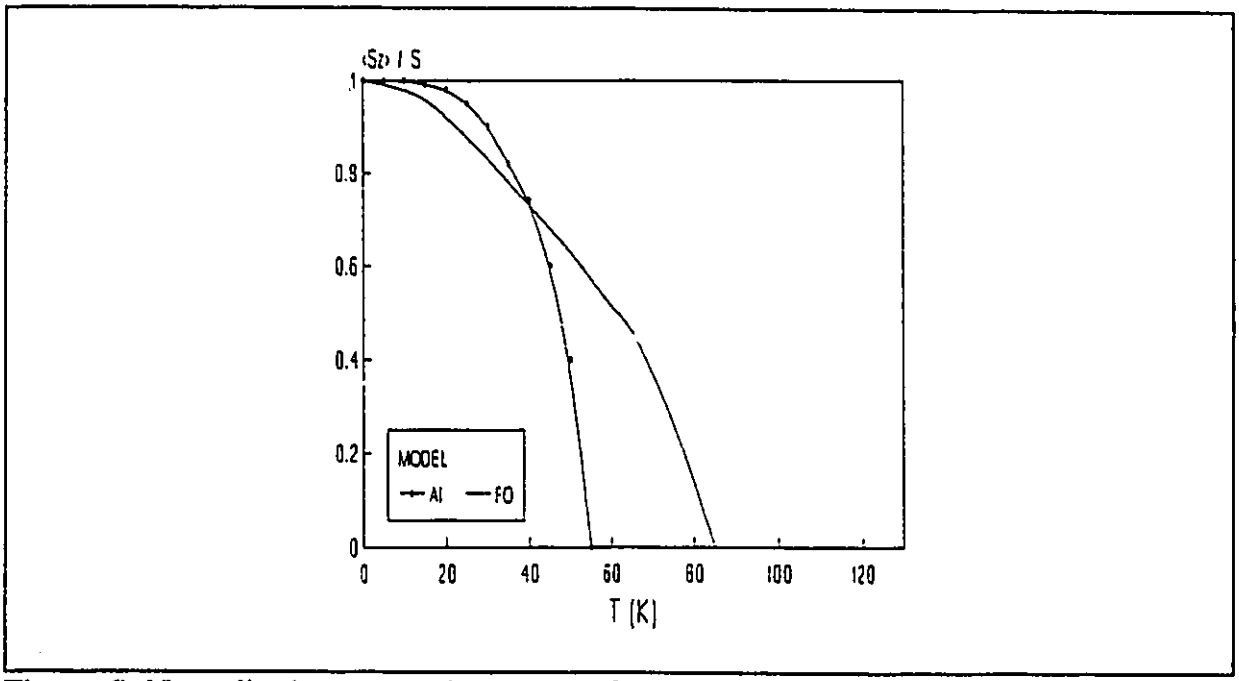


**Figure 6b** Normalized average spin per atom for FO and AI models. Parameters as in fig.6a.

## 4.2 THE PHASE DIAGRAM

### 4.2.1 The Curie Temperature

The Curie temperature may be derived from Eq.(30) by invoking the small argument expansion of the Brillouin functions and insisting that the slope of each equation equal 1. The result is:

$$T_C = \frac{-b + \sqrt{b^2 - 4c}}{2} \tag{33}$$

with:

$$b = -\left(\sum_{n=0}^{z} nP(n)\right)\alpha J_{AA} + \left(\sum_{n=0}^{z} (z-n)\,P(n)\right)6J_{BB}$$

$$c = \left(\sum_{n=0}^{z} nP(n)\right)\left(\sum_{n=0}^{z} (z-n)\,P(n)\right)\alpha 6 J_{AA}J_{BB} - \left(\sum_{n=0}^{z} nP(n)\right)\left(\sum_{n=0}^{z} (z-n)\,P(n)\right)\alpha 6 J_{AB}^2, \tag{34}$$

and:

$$\alpha = \frac{S^A(S^A+1)}{3k_B}, \quad 6 = \frac{S^B(S^B+1)}{3k_B}. \tag{35}$$

At 100 at%$A$ or $B$ this expression reduces to Eq.(20).

### 4.2.2 Typical Phase Diagrams

The plot of Curie temperature vs. alloy composition provides a *phase diagram* for the system identifying the regimes of paramagnetic and ferromagnetic behaviour. The shape of the phase diagram depends on the exchange constants and the spin quantum numbers, however for $J$ all positive the basic topology remains the same.

Figs.7a and 7b illustrate diagrams for several choices of $J_{AA}$, $J_{AB}$ and $J_{BB}$.

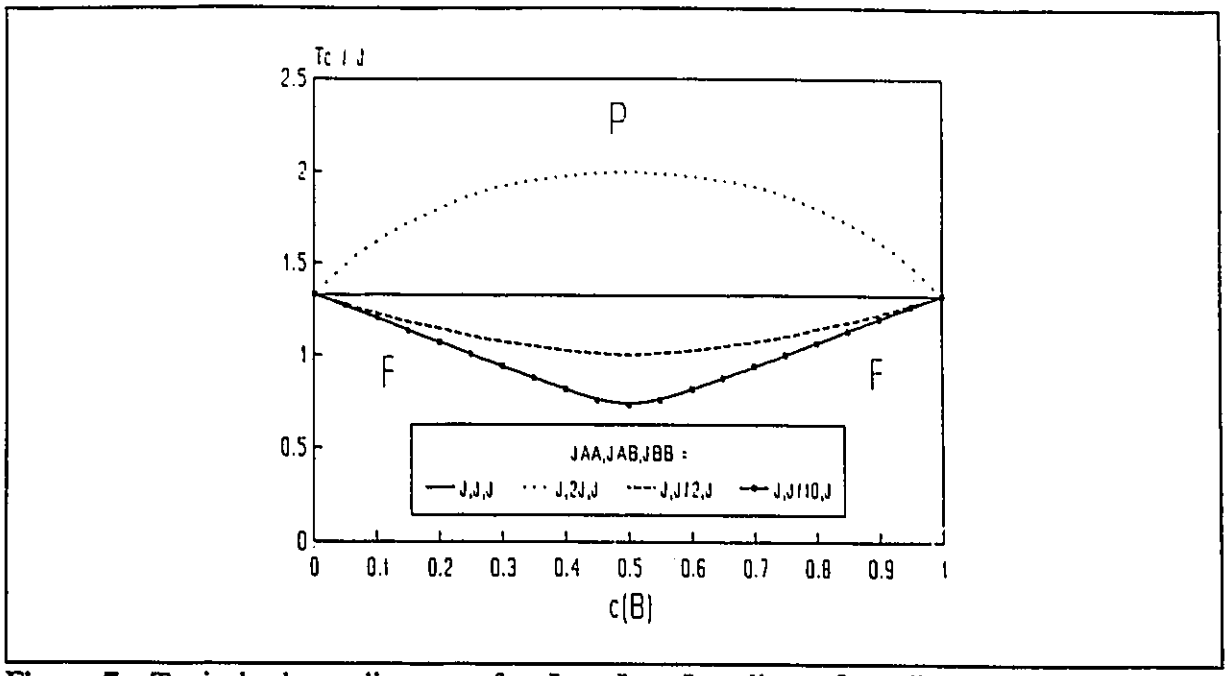


**Figure 7a** Typical phase diagrams for $J_{AA}$, $J_{AB}$, $J_{BB}$ all > 0. The curve separates the paramagnetic regime from the ferromagnetic regime in zero applied field.

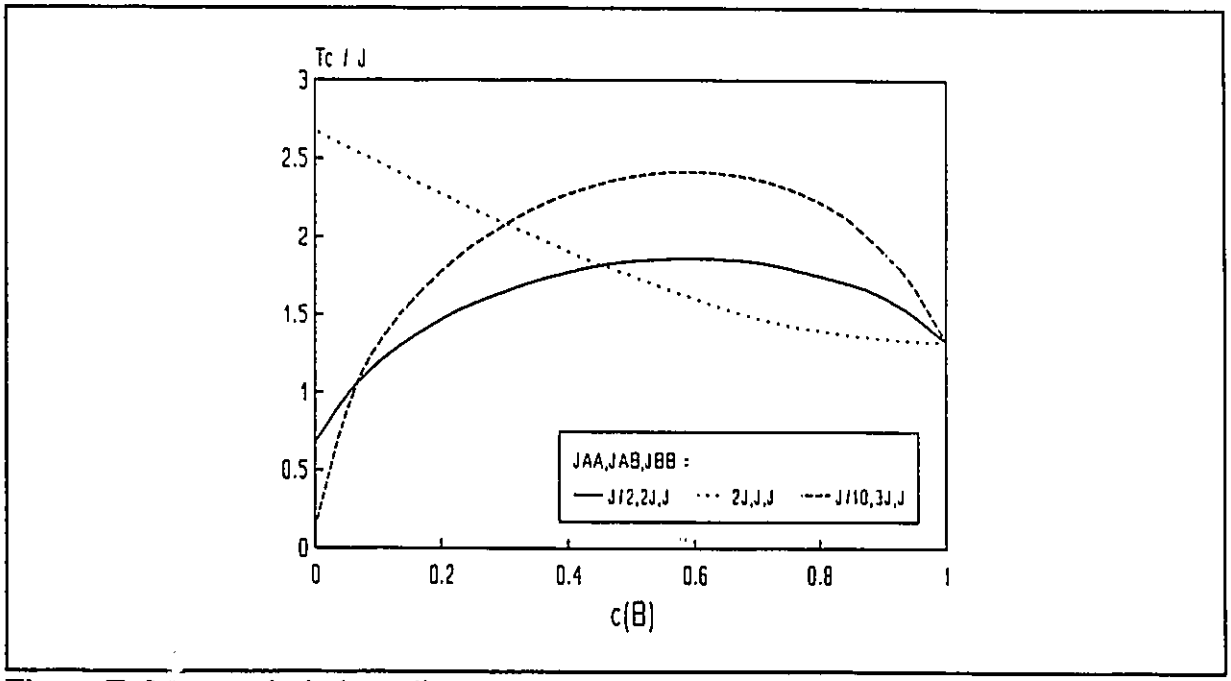


**Figure 7b** More typical phase diagrams.

The Curie temperatures are, except for end members, higher than those found by applying the AI model for the same set of parameters. This is illustrated by a specific case in fig.7c.

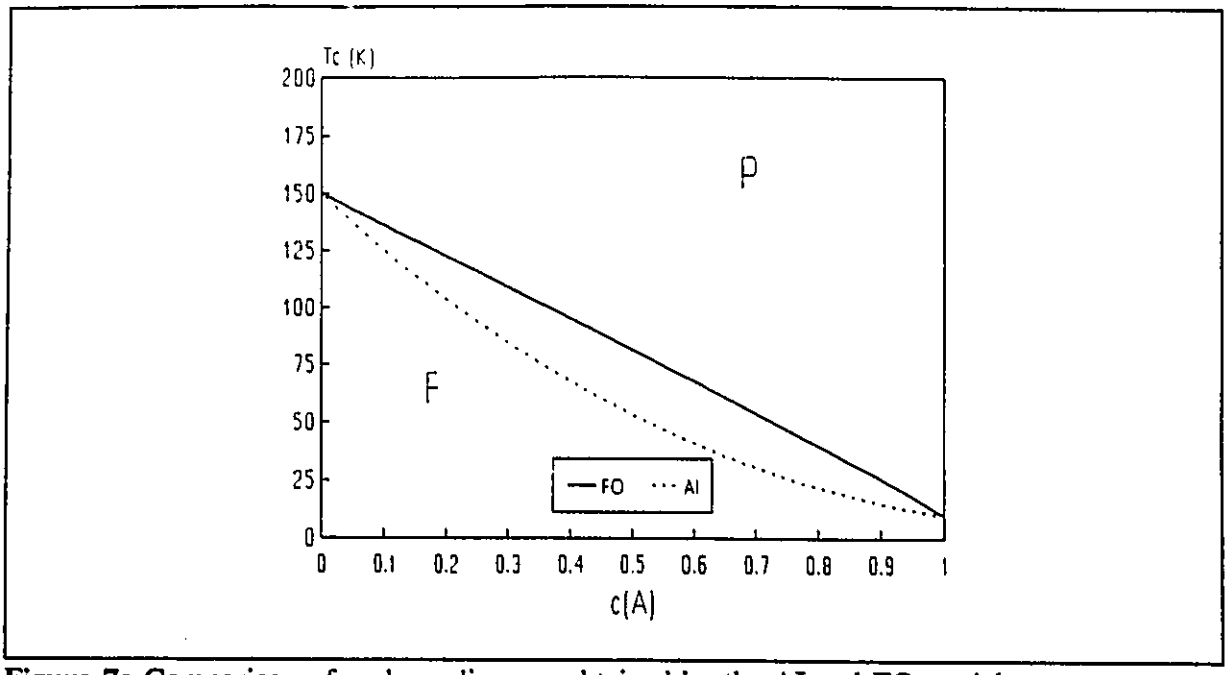


**Figure 7c** Comparison of a phase diagram obtained by the AI and FO models. $S^A = 0.5$, $S^B = 1.5$, $J_{AA} = 20K$, $J_{AB} = 40K$, $J_{BB} = 60K$.

Having achieved a model which reproduces key experimental features of the systems we are studying, we have pursued two distinct branches of research stemming from it. We have (1) pursued higher order class models in the case of a 1-D chain and (2) applied the FOC model to a real well known system, namely the fcc Fe-Ni alloys.

# 5/ HIGHER ORDER CLASSES IN 1-D

## 5.1 THE SECOND ORDER CLASS MODEL

### 5.1.1 Class Structure

We start the analysis of the 1-D chain alloy by recalling the FOCs for an *A*-type atom, illustrated in fig.7.

To improve our model we subdivide these classes. We identify the nearest neighbours of a spin according to *their* FOC and thus create Second Order Classes (SOCs). In order to do this we need to know the identity of the *second* nearest neighbours. There is no general way to enumerate the SOCs so we will adopt an arbitrary labelling scheme. SOC *A,n,m* contains the spins of species *A* which have *n A*-type nearest neighbours, *m* ranges from 1 to 4. The SOCs for FOC *A,2* are illustrated in fig.8.

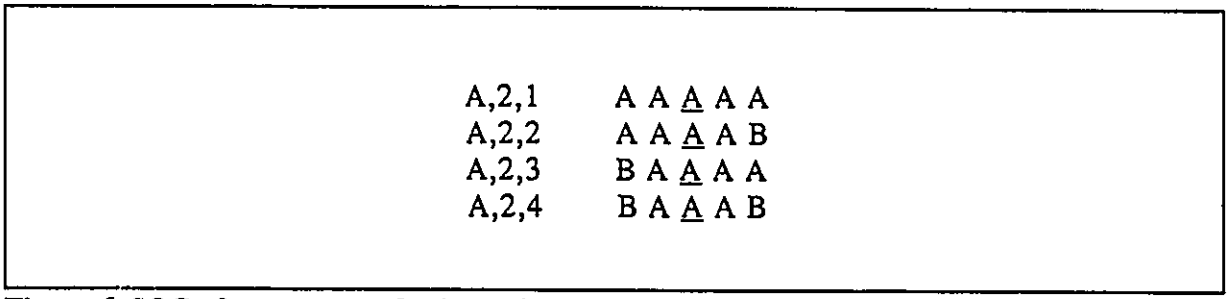


**Figure 8** SOCs for an atom of FOC *A*,2

### 5.1.2 Constructing the Mean Field

We see that, for instance, a spin in the SOC *A,2,4* has nearest neighbours which are both of the FOC *A,2* by virtue of having two *A*-type atoms in the first coordination shell. As in the FOC model, it is the nearest neighbours which define the mean field for the central spin of a class. For instance, for a spin of SOC *A,2,4* the mean field is:

$$\overline{H}_{A,2,4} = 2\frac{J_{AA}}{g\mu_B} S_z^A \langle \overline{S}_z^{A,2} \rangle . \qquad (36)$$

### 5.1.3 Spatial/Thermal Average Spin Calculations

The spatial/thermal average spin, for instance that pertaining to FOC *A,2* is calculated as follows:

$$\langle \overline{S}_z^{A,n} \rangle = \sum_{m=1}^{4} P(m) \langle S_z^{A,n,m} \rangle . \qquad (37)$$

Each term is weighted with the probability of such a class. For instance, the probability for $m = 1$ is always determined by the presence of two *A*-type spins in the second coordination shell so that $P(m=1) = c(A)^2$. There are six FOCs and therefore six equations like Eq.(36) in six unknowns. The equations are solved numerically as described in Appendix II. The resulting FOC averages for species *A*, for a particular example, are shown in fig.9a.

The species spatial/thermal average is computed by summing over the three species FOCs as in Eq.(29). For instance, for *A*-type spins:

$$\langle \overline{S}_z^{A} \rangle = \sum_{n=0}^{2} P(z,n) \langle \overline{S}_z^{A,n} \rangle . \qquad (38)$$

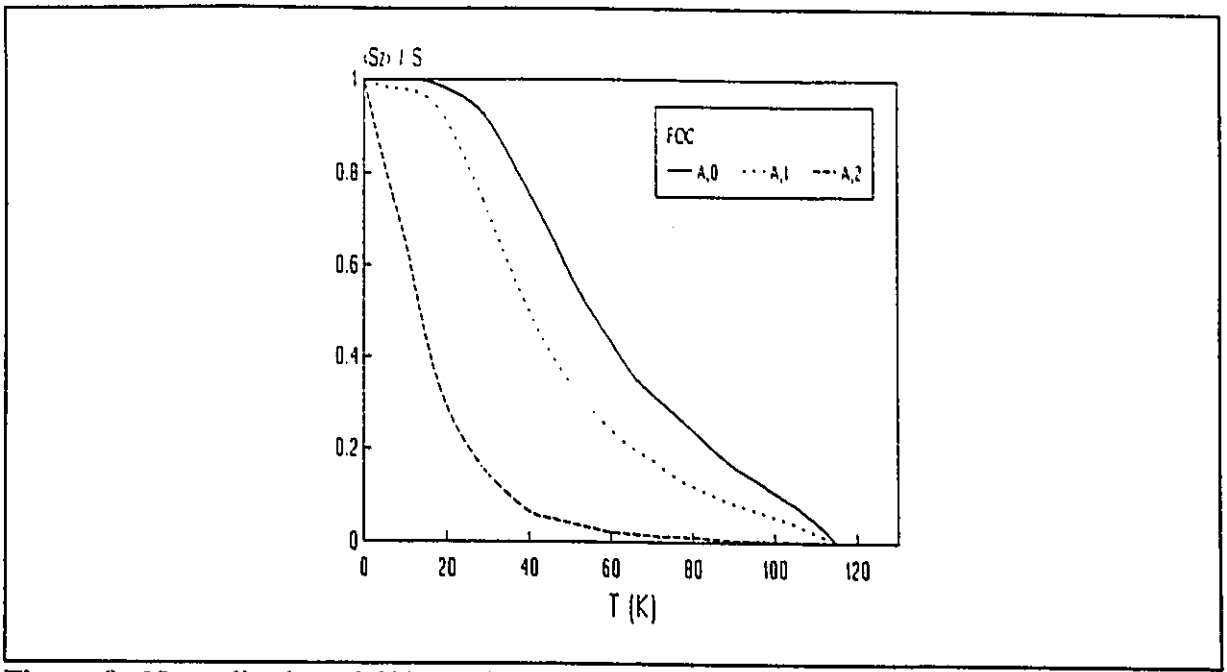


**Figure 9**a Normalized spatial/thermal averages for the three FOCs of species A as a function of temperature. $S^A = 0.5$, $S^B = 1.5$, $J_{AA} = 20K$, $J_{AB} = 40K$, $J_{BB} = 60K$.

The resulting average, as a function of temperature, is shown for species *A* in fig.9b : long with that from the FOC model.

The total system average spin is computed as in Eq.(32). In fig.9c the result is compared with that from the FOC model, the Ordered Alloy model and the Average Interaction model.

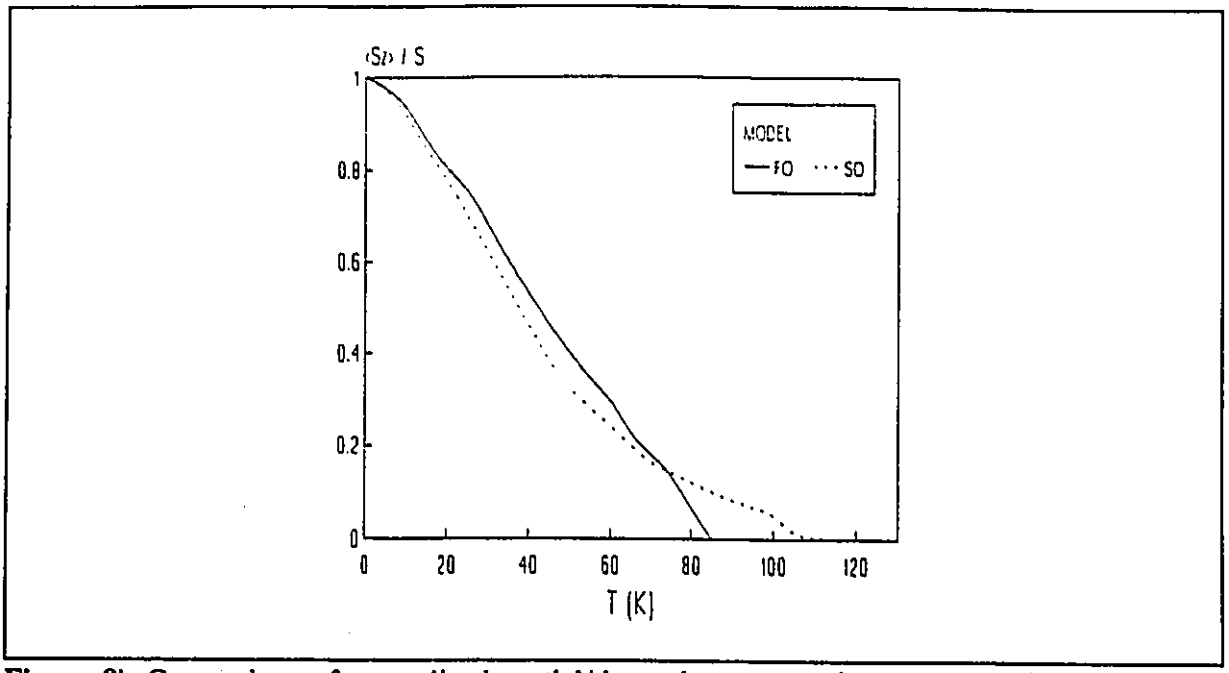


**Figure 9b** Comparison of normalized spatial/thermal average spin *per atom of species A* as a function of temperature obtained by SO and FO models. Parameters as in fig.9a.

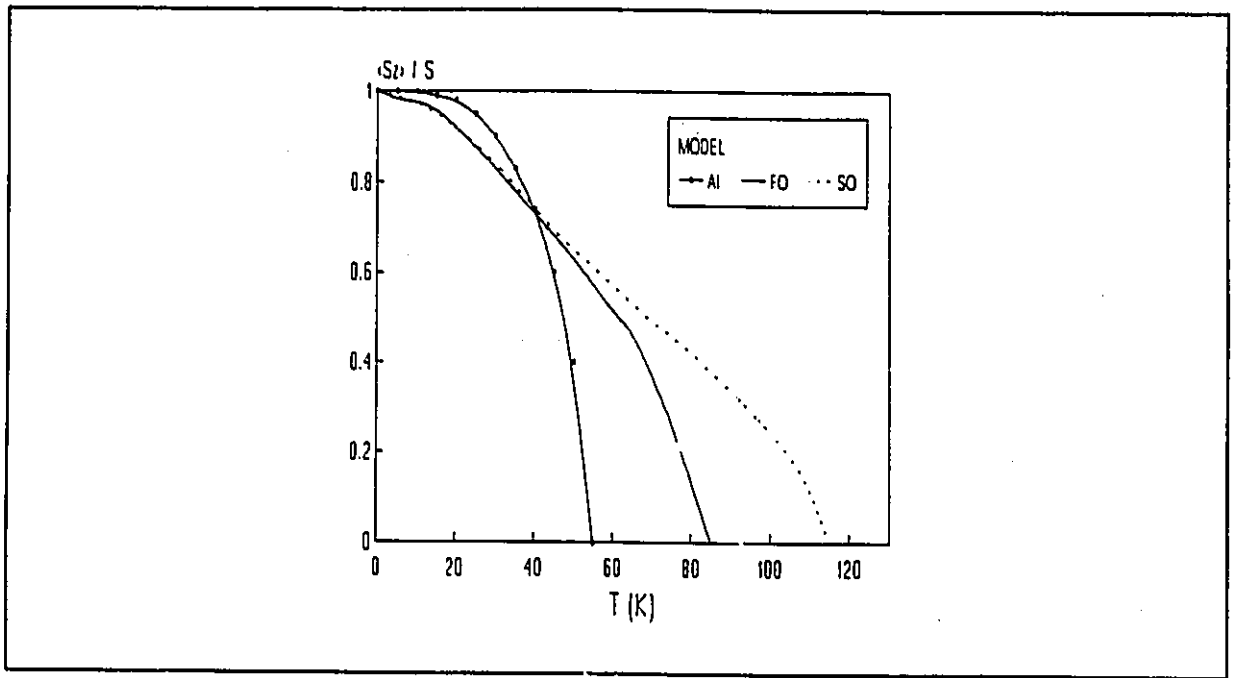


**Figure 9c** Comparison of normalized average spin *per atom* as a function of temperature obtained by SO, FO, and AI models. Parameters as in fig.9a.

We see that the curves become successively more flattened as the level of detail acknowledged by the model increases while the Curie temperature calculated becomes higher. This result is quite general.

### 5.1.4 The Curie Temperature

As in our previous models we invoke a small argument expansion to reduce our Brillouin functions to linear equations. Six linear equations, one for each FOC, result and may be described by a six by six matrix of coefficients. The condition that a non-trivial solution exists is imposed by insisting that the determinant of the matrix equals zero. By computing the determinant numerically for a series of temperatures $T_C$ may be found. In practice it is easier to vary the temperature, solving the original system of equations at each point until the spin averages vanish.

## 5.2 THE THIRD ORDER MODEL

The next step in the refinement of our model is to further narrow the definition of similar local environments. We identify the nearest neighbours according to their SOC and define a Third Order Class (TOC) to include only those spins which have the same number of each SOC in the first shell. In order to do this we need to know the identity of the *third* nearest neighbours of the spin in question. We find ninety-six TOCs. By summing over these classes as in Eq.(36) we arrive at twenty-four equations in twenty-four unknowns. Because these equations are non-linear, finding a solution by iteration is non-trivial. We solve the system of equations; however, the cost in terms of computer time is much greater.

The results, shown in fig.10a, for the average spin per atom, demonstrate further convergence with respect to the simpler models. Appendix V contains another example.

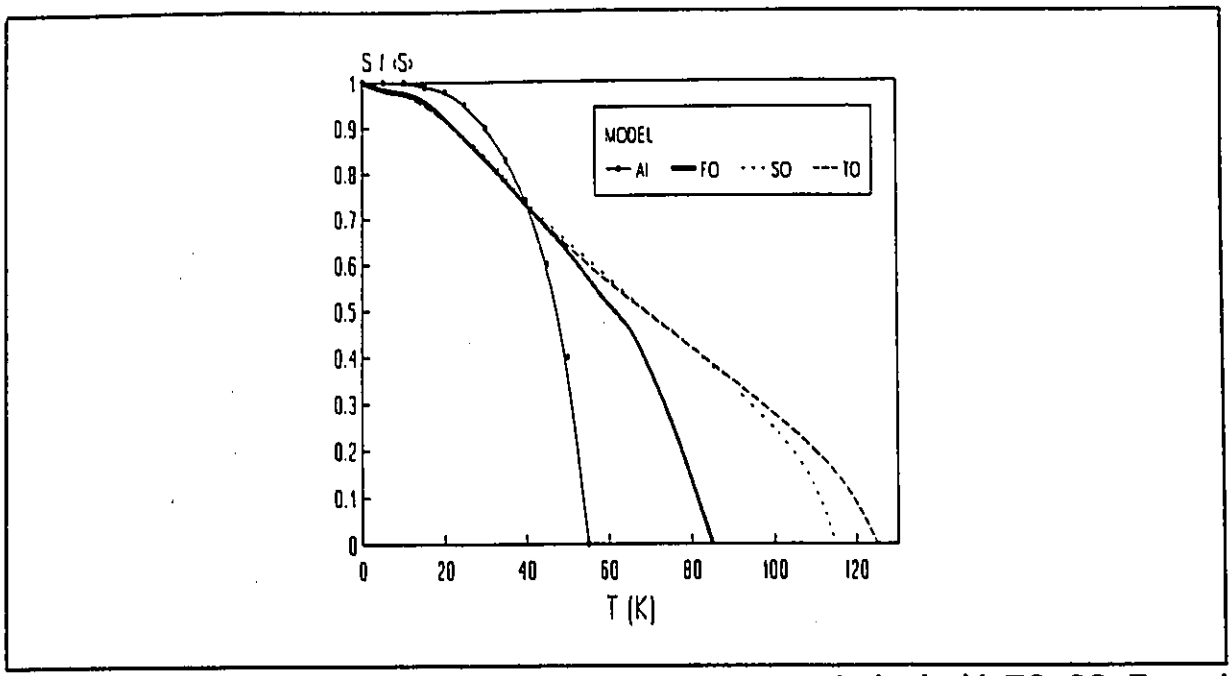


**Figure 10a** Normalized average spin *per atom* vs. temperature obtained with TO, SO, Fo, and AI models. Parameters as in fig.9a.

The increased flattening of the magnetization curves is emphasized by plotting against reduced temperature as in fig.10b. The flattening can be understood in terms of randomness, this phenomenon is discussed in Chapter 6.

Finding the determinant of a 24x24 matrix in order to find the Curie point is, in practice, difficult. Instead, $T_C$ is interpolated from the average spin vs. temperature curve. The further convergence of the Curie temperature as the model complexity increases is illustrated in fig.10c. The line drawn in the diagram is included for emphasis only.

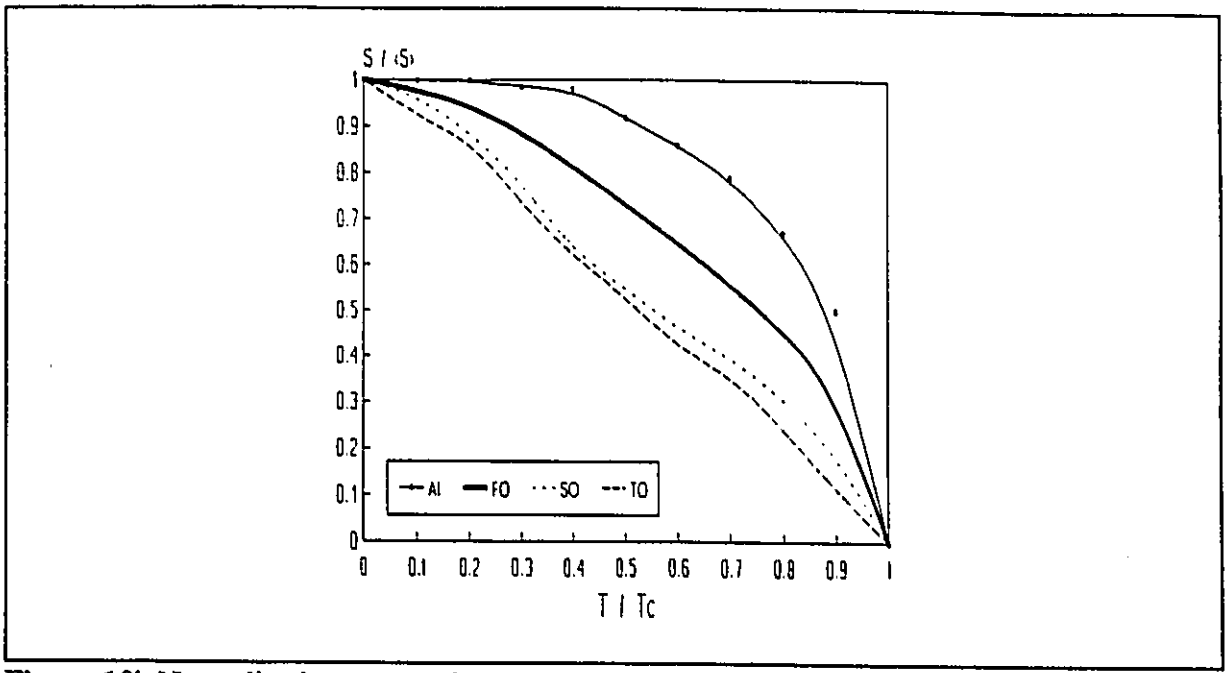


**Figure 10b** Normalized average spin *per atom* vs. reduced temperature obtained by TO, SO, Fo and AI models. Parameters as in fig.9a.

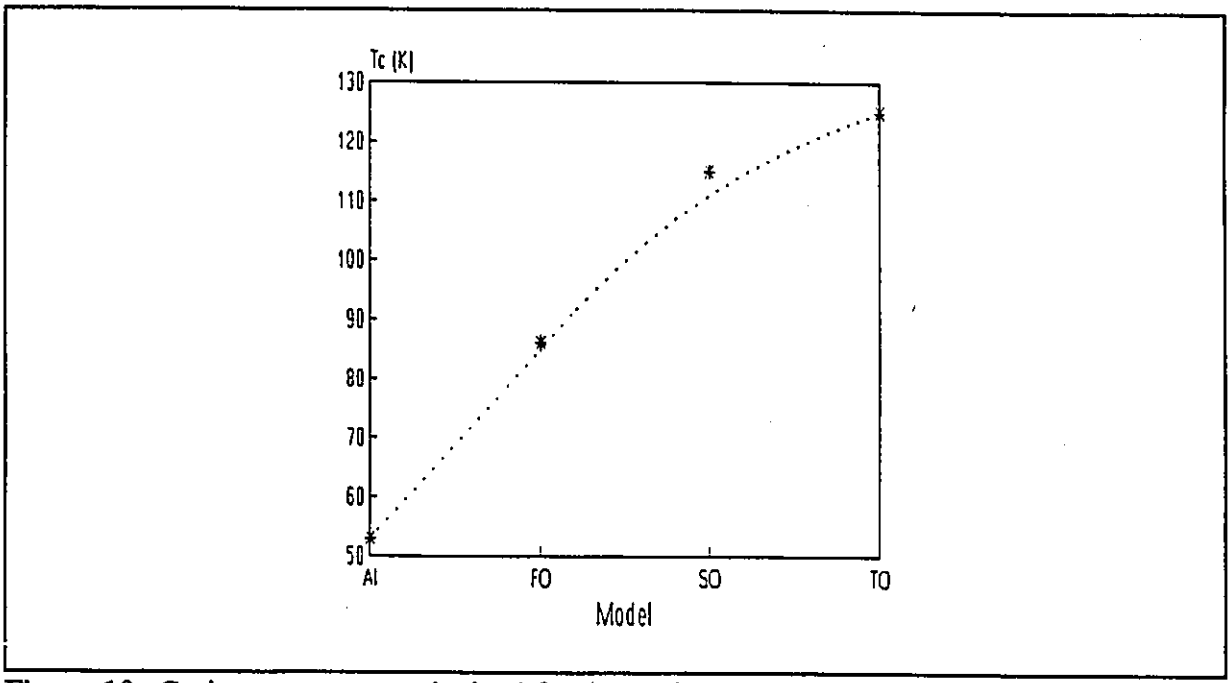


**Figure 10c** Curie temperatures obtained from TO, SO, FO and AI models.
$J_{AA}$ = 20K, $J_{AB}$ = 40K, $J_{BB}$ = 60K, $S^A$ = 0.5, $S^B$ = 1.5, c(A) = 50 at%.

## 5.3 SUMMARY OF THE CLASSIFICATION MODELS

The extension of the model from First through Second to Third Order Classes is summed up in

Table 1 below. Note that even as we extend our consideration to next nearest neighbours and beyond, we follow the same process in each case. We classify spins according to the identity of their nearest neighbours and construct a mean field for each class accordingly. Each model is named according to the coordination shell needed for the determination of the classes.

While remaining conceptually simple at every stage, the calculational difficulty increases dramatically as the number of variables increases. For the 1-D chain this number, two for the FO model, rises to six and then to twenty-four. The next step, the Fourth Order Model would involve ninety-six unknowns and 384 classes. Although these numbers are very much less than $N$, we have seen significant convergence. For the 1-D model then there is no need to compromise on quality of results as the mathematics remain easily accessible at every level.

In the case of a 2-D square lattice however, applying even the SO model requires over two hundred classes comprising twelve equations in twelve unknowns. There is no simple method of enumerating these classes and calculating probabilities. The 3-D fcc lattice ($z$=12), at the SO level, has hundreds of classes and twenty six unknowns. The problem of identifying each class in order to construct a mean field and calculating the probability of finding a spin of such a class is enormous and was not attempted for this project.

| Model | Results Obtained (No. of Eqs.) | Ex. | Classes defined | Ex. | Mean fields depend on: |
|---|---|---|---|---|---|
| AI | Thermal average spin per atom (1) | $<S_z>$ | all spins are in the same class | | See Results obtained |
| FO | ZOC (species) specific spatial/thermal average spin (2) | $<\bar{S}_z^A>$ | First Order (6) | *A,1*<br>A<u>A</u>B<br>*B,0*<br>B<u>B</u>B | " |
| SO | FOC specific spatial/thermal average spin (6) | $<\bar{S}_z^{A,n}>$ | Second Order (24) | *A,1,2*<br>BA<u>A</u>BA<br>*B,0,4*<br>AB<u>B</u>BA | " |
| TO | SOC specific spatial/thermal average spin (24) | $<\bar{S}_z^{A,n,m}>$ | Third Order (96) | *A,1,2,3*<br>ABA<u>A</u>BAB<br>*B,0,4,2*<br>BAB<u>B</u>BAA | " |

Table 1. Summary of Class Structure.

# 6/ THE EFFECT OF DISORDER

## 6.1 THE ORDERED ALLOY MODEL

In the interests of determining the impact of randomness on the properties of the alloy we employ the example of an Ordered Alloy (OA) with species occurring in the ratio 1:1. By arranging them in a specific manner we have a ferrimagnet with the same probabilities for the three types of interactions as does the random magnet. For instance, a 1-D alloy would be arranged as in fig.11.

$$\cdots A\,A\,B\,B\,A\,A\,B\,B\,A\,A\,B\,B\,A\,A\cdots$$

**Figure 11** Our 1-D ordered alloy.

There are two sublattices, each one associated with a particular type of atom. The spins on one sublattice have a mean field in common, one that is dependent on both sublattice spin averages.

The mean fields for an *A*-type atom and a *B*-type atom are:

$$\overline{H}_A = 2\frac{J_{AA}}{g\mu_B}\langle S_z^A\rangle + 2\frac{J_{AB}}{g\mu_B}\langle S_z^B\rangle$$

$$\overline{H}_B = 2\frac{J_{AB}}{g\mu_B}\langle S_z^A\rangle + 2\frac{J_{BB}}{g\mu_B}\langle S_z^B\rangle . \qquad (39)$$

With these fields used in the calculation of thermal averages for each sublattice we arrive at two equations in two unknowns:

$$\langle S_z^A \rangle = S^A B_{S^A}(2\beta J_{AA} S^A \langle S_z^A \rangle + 2\beta J_{AB} S^A \langle S_z^B \rangle)$$
$$\langle S_z^B \rangle = S^B B_{S^B}(2\beta J_{AB} S^B \langle S_z^A \rangle + 2\beta J_{BB} S^B \langle S_z^B \rangle) . \quad (40)$$

The solution of these equations yields temperature dependent results for each type of atom and, by combining these as in Eq.(31), we find the total average spin. A plot of average spin vs. temperature for particular parameters is shown in comparison with that resulting from the FO model in fig.12.

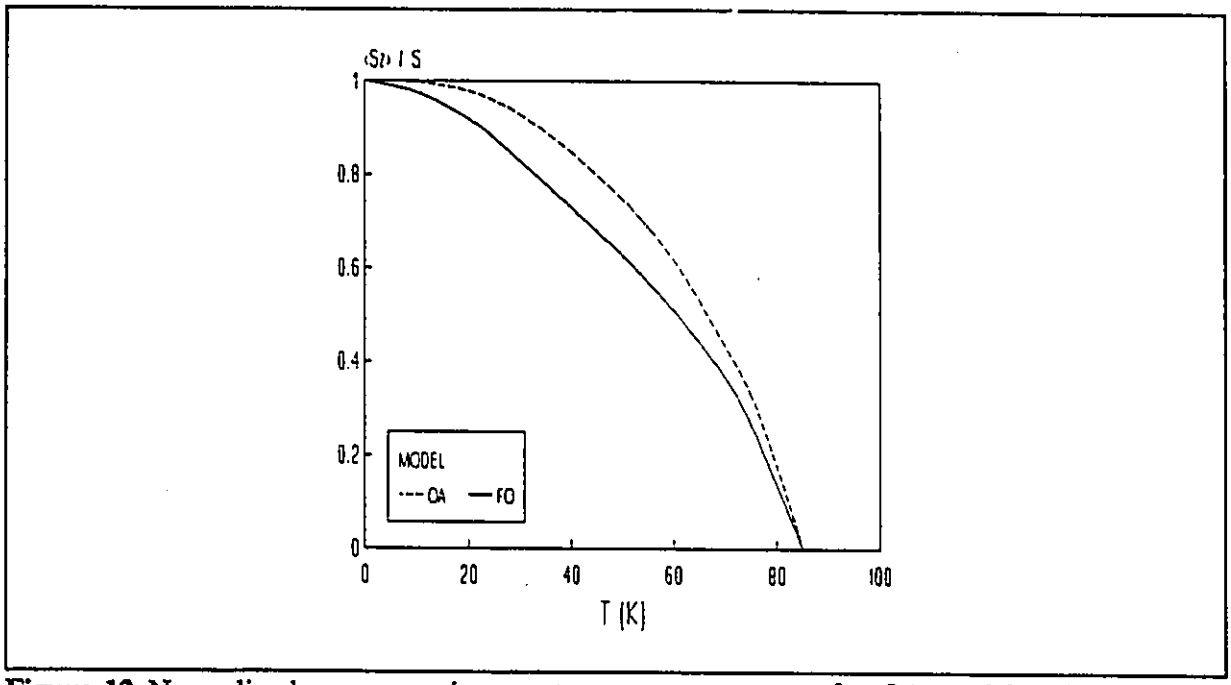


**Figure 12** Normalized average spin per atom vs. temperature for OA model and FO model. Parameters $J_{AA}$ = 20K, $J_{AB}$ = 40K, $J_{BB}$ = 60K, $S^A$ = 0.5, $S^B$ = 1.5, c(A) = 50 at%..

## 6.2 THE EFFECT OF RANDOMNESS ON THE MAGNETIZATION CURVE

Fig.12 shows that randomness has a significant impact on the properties of a system. The curves have a different temperature dependence. The effect can be understood in terms of the presence of clusters of like spins in the random alloy. The specific example we have used in the figures above ($J_{AA}$=20K, $J_{AB}$=40K, $J_{BB}$=60K, $S^A$=0.5, $S^B$=1.5) can be use to illustrate this phenomenon. Atoms of type $A$ would on their own order below 10K[8]. In the random magnet those atoms of type $A$ which have same species neighbours ($\cdot AAA \cdot$) tend towards disorder at temperatures at which the system is, on the whole, still ordered. These atoms have spin averages which are depressed with respect to their saturation value to a greater degree than spins in other local environments and of other species. These therefore lower the overall average leading to the characteristic flattening.

This effect is more pronounced in our higher order models. In the FO model these depressed spin averages are included in the total species spin average which in turn engenders the mean field. The mean field is at once lowered by having the smaller spins included and, for an $A$-type atom with $A$-type neighbours, elevated with respect to that found in the pure substance at the same temperature. This ensures that the spin thermal averages are still relatively high. In a higher order model the $A$-type atom with same species nearest neighbours feels a more appropriate mean field. This mean field is constructed not of the overall species average spin but only that average over other $A$-types with at least one other $A$-type nearest neighbour. This mean field is therefore smaller than that in the FO model and the result is further depression of the thermal average spin. The higher order the model, the more the tendency of spins in certain configurations to pursue their pure substance behaviour is revealed.

---

[8] Eq.(20) with $S$ = 0.5 and $J$ = 20K.

## 6.3 THE EFFECT OF RANDOMNESS ON THE CURIE POINT

### 6.3.1 Curie Point for the OA Model and FO Model

We can calculate the Curie temperature for the ordered alloy by taking the small argument expansion of each Brillouin function and insisting that the slope of each resulting line equals 1. We find:

$$k_B T_C = \frac{-b + \sqrt{b^2 - 4c}}{2} \tag{41}$$

where:

$$b = \frac{S^B(S^B+1)}{3} J_{BB} - \frac{S^A(S^A+1)}{3} J_{AA}$$
$$c = \frac{S^A(S^A+1)\, S^B(S^B+1)}{9} J_{AB}^2. \tag{42}$$

The Curie point thus determined is exactly the same for the FO model. The similarity between these two models is that each employs two equations in two unknowns. In both cases the mean field is constructed from two average spins, one for each species. Clearly this is a determining factor in the estimate of the Curie point.

### 6.3.2 The Curie Point for Higher Order Models

The estimate of the Curie temperature is higher in the higher order models. This is the result of the presence of mixed atom clusters in which $A$-type spins have $B$-type neighbours. These spins maintain a finite thermal average at temperatures well above their intrinsic Curie point. The fact that the effect is more pronounced in higher order models is understood following the same reason applied to the flattening of magnetization curves above.

Thus the system tends toward a Curie temperature determined by the presence of the $B$-type atoms ($T_C = 150$K) while having a lowered average spin per atom determined by the presence of $A$-type atoms.

# 7/ APPLICATION TO A REAL SYSTEM

A number of modifications to our models must be made in order to treat a real system. A summary of the assumptions made thus far (Section 7.1) lays the foundation for the generalization of our models for application to systems in which (1) the alloy is atomically disordered but not perfectly random, (2) itinerant electrons lead to non-half-integral effective moments, (3) some exchange constants favour antiferromagnetic ordering and (4) interactions persist beyond the first coordination shell. The procedure for calculating the experimentally measurable properties of a real system is outlined in Section 7.6. In Chapter 8 these calculations are performed for the fcc Fe-Ni alloys which have features (2) and (3).

## 7.1 BASIC ASSUMPTIONS OF OUR MODEL

Although the exchange constant is a function of the lattice parameter, which is in turn a function of temperature, we have, as a first approximation, assumed these constants to be fixed.

We consider that spin alignment is unhindered by crystalline anisotropy. We assume that no spins have non-zero averages for x and y components. In an alloy with only ferromagnetic interactions this is a good assumption.

The implications of the situation in which some bonds are antiferromagnetic are discussed in Section 7.4.

We consider each ion to be in its electronic ground state, excited states being inaccessible at the temperatures which we are considering. We take orbital angular momentum to be *quenched* so that only spin contributes to the magnetic moment.

## 7.2 IMPERFECT RANDOMNESS

The ferrimagnetic case of perfect ordering of alloy components on the lattice and the case of perfectly random arrangement of these components are extremes. In general, an alloy may be atomically ordered to any degree, with large or small fluctuations from the most energetically favourable mutual positioning of species, according to conditions of temperature or sample preparation (quenching etc.). These cases are more difficult because there is, in general, no simple way of computing the probabilities of finding an atom of one species on a site given the identity of its near neighbours.

The probability may be arrived at by applying statistical techniques such as mean field theory to the ordering of atoms. Once an expression for $P(A,z,n)$ has been reached, by whatever means, the mechanics of applying our mean field technique are the same as for the identically random case.

## 7.3 ITINERANT ELECTRONS

In the case of metallic alloys (such as Fe-Ni) the presence of itinerant electrons leads to an average spin quantum number that is non-half integral. For instance, experiment reveals that the moment for Ni atoms in pure nickel is $0.6\mu_B$ implying $S^{Ni} = 0.3$. For the Fe atoms we have assumed a moment of $2.8\mu_B$ or $S^{Fe} = 1.4$. This is based on the extrapolated endpoint of the Slater-Pauling curve for the alloys in this series (fig.13). The moment carried by each atom in pure Fe is not considered because it occurs in a bcc form.

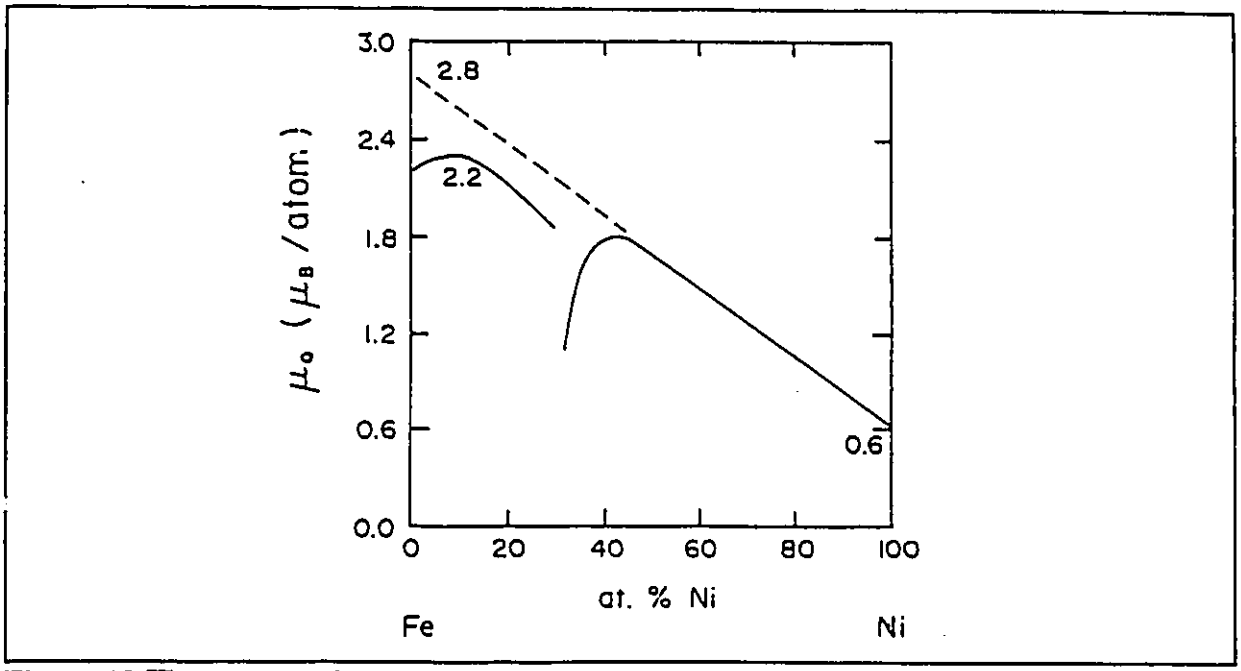


**Figure 13** The measured spontaneous moment per atom at T=0, showing extrapolation to the effective moment on Fe. [3].

We incorporate these facts by assigning to each atom of a particular species one of two half-integral spin quantum numbers in such a proportion that the spatial average is that non-half-integral number known through experiment. In this way we have replaced time fluctuations with spatial fluctuations. This substitution is also reasonable if we interpret the spin-spin interaction as occurring between average moments with an effective $S$. In the case of Fe we consider some of the atoms to be spin 1.5 and some 1.0 as follows:

$$\langle S_z^{Fe} \rangle = \tau \langle S_z^{Fe} \rangle_{S=1.5} + (1-\tau) \langle S_z^{Fe} \rangle_{S=1.0} \qquad (43)$$

with $\tau = 0.8$.

## 7.4 MIXED EXCHANGE

### 7.4.1 Implications for Real Systems

Alloys whose cooperative magnetic behaviour is governed by exchange constants of both ferro- and antiferromagnetic nature are known as mixed exchange systems and are often subject to interesting effects due to the competing forces of parallel and antiparallel alignment. In some cases atoms cannot hope to satisfy all of their bonds, a situation known as *frustration*. These considerations are important in Fe-Ni since $J_{FeFe}$ is negative, while $J_{FeNi}$ and $J_{NiNi}$ are positive

Recall that the thermal average moment on an atom is the result of energy considerations favouring a certain orientation with respect to its neighbours. Our spins, which have a Heisenberg type interaction with one another, have interactions in the x and y directions. Preferred states are those in which these bonds are satisfied. Spins may compensate for the competition between parallel and antiparallel alignment by developing finite thermal averages in the x and y directions. The spin, exploiting three degrees of freedom in seeking a lowest energy state, is said to be *canted* with respect to the z direction.

### 7.4.2 Impact on Mean Field Equations

In the mean field picture, the result of mixed exchange is a mean field which is not in the same direction throughout the solid. Our approach is not designed to handle this. Instead, our spins exhibit depressed z direction components as evidence of canting. In practice, mixed exchange causes the Brillouin function to deviate significantly from its purely ferromagnetic form. By comparing functions at the same temperature but different concentrations of $B$ (fig.14), where $J_{BB}$ is the only antiferromagnetic exchange constant, it is seen from the position of the intersection that the solution is much lower in the $B$ rich case. Thus, the inability of the spin to satisfy its z direction relationship results in a lowered component in that direction, leaving room for finite average spin components in the other directions.

We note also that in the case of 100% $B$ the Brillouin function is just the x-axis reflection of a normal ferromagnetic one. There is no true solution in this case but the intersection of the function with the line y = -x suggests the existence of an antiferromagnetic pseudo-solution. In other words, in this regime, the response to a *positive* mean field is a *negative* thermal average and vice versa. We interpret this to mean that the system would order antiferromagnetically, that is to say that every spin would have an antiparallel orientation with respect to its nearest neighbours with the thermal average on every spin having the same magnitude. The Néel temperature $T_N$ is the antiferromagnetic analog of the Curie temperature. The temperature we find for the appearance of this pseudo-solution on cooling is the same as the $T_N$ derived using the same parameters from a proper sublattice treatment of the antiferromagnet[9], thereby supporting our interpretation.

---

[9] See Appendix II for this calculation or Smart [2] for more about antiferromagnetic systems and the standard MFT approach.

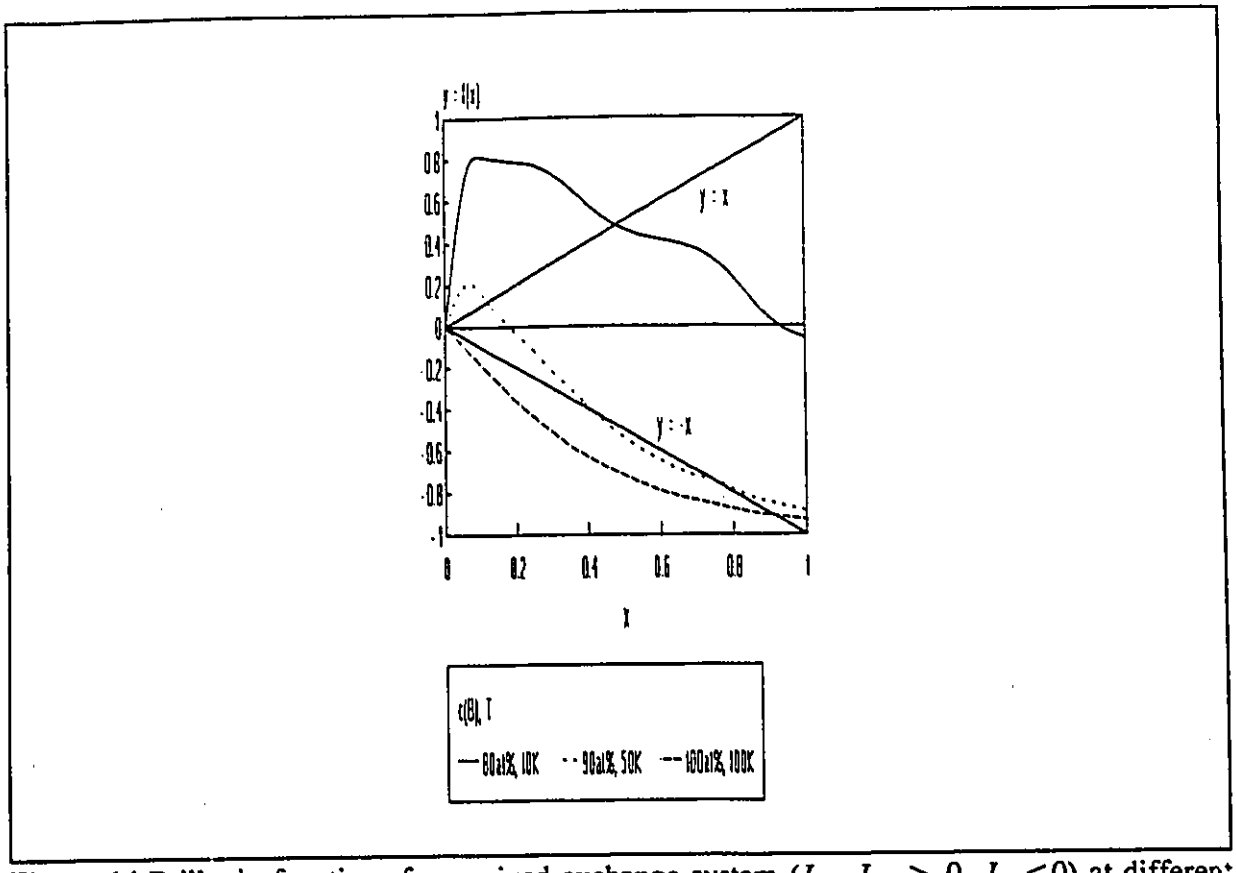


**Figure 14** Brillouin functions for a mixed exchange system ($J_{AA}$, $J_{AB} > 0$, $J_{BB} < 0$) at different temperatures and concentrations.

### 7.4.3 Phase Diagram for a Mixed Exchange System

The Brillouin function for *B*-rich member alloys often intersects with both y = x and y = -x, suggesting the existence of *both* types of ordering and two transition temperatures. This is illustrated by a sample phase diagram for a mixed exchange system in fig.15.

The implied existence of more than one type of ordering at a given composition is an artifact of our MFT approach and may not have any physical counterpart. Our model is believed to deal well with low concentrations of antiferromagnetic components. Our Néel temperature line in the phase diagram probably marks the boundary of the regime in which the model may be used with confidence.

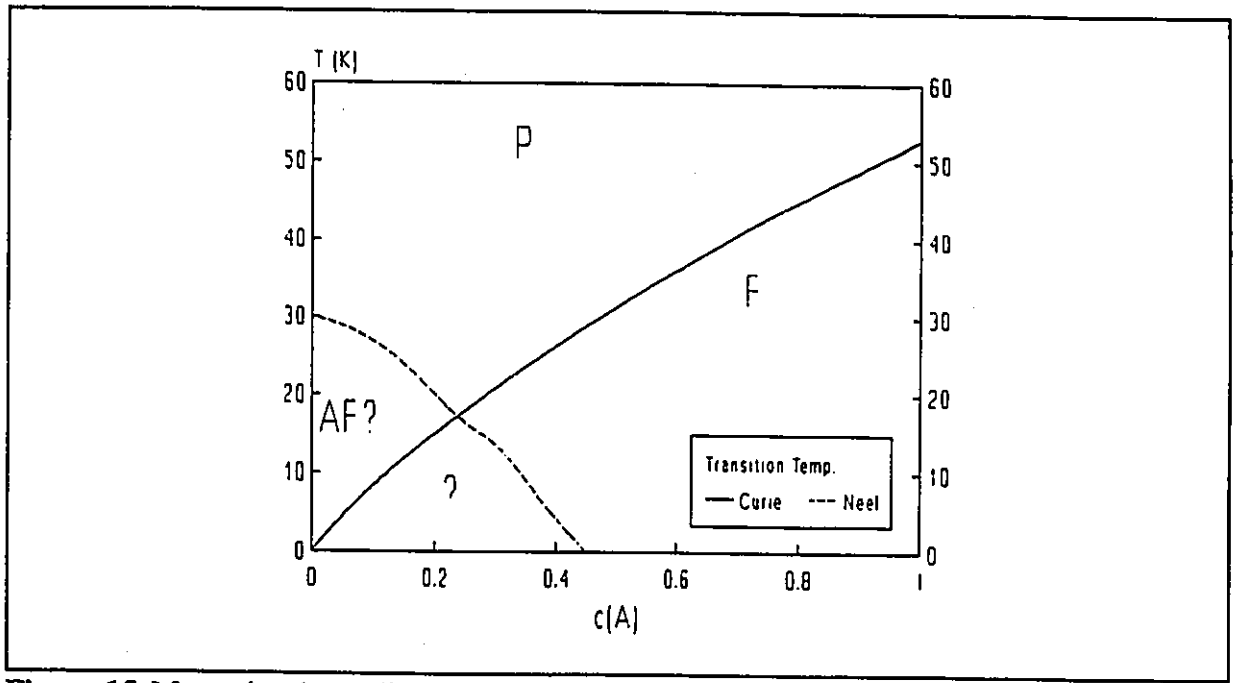


**Figure 15** Magnetic phase diagram for a typical mixed exchange system. ($S^A=S^B=1$, $J_{AA}$, $J_{AB} > 0$, $J_{BB} < 0$)

## 7.5 INTERACTIONS BEYOND THE FIRST COORDINATION SHELL

In Section 2.1.1 we asserted that our approach could be extended if necessary to systems in which exchange interactions between non-first-nearest-neighbours are important. Again, the trick is in constructing an appropriate mean field. Such a mean field depends on the thermal average spins of second nearest neighbours etc. Our FOCs would depend on the identity of both the first and second nearest neighbours. The greater number of possible configurations would therefore increase the number of such classes. The principle of summing over the thermal average for each class of spin in order to find the species average still applies and the result would still be two equations in two unknowns.

## 7.6 PROCEDURE FOR MODELLING A REAL SYSTEM

In order to calculate the properties of a real system we must first know the parameters of spin quantum numbers and exchange constants. The spin quantum numbers may be inferred from the Slater Pauling curve as in Section 7.3. Our strategy for finding the three exchange constants $J_{AA}$, $J_{AB}$ and $J_{BB}$ involves calculating one physical property (transition point as a function of composition) and fitting it to experimental data, a process described in Section 8.3.1. With these five parameters in hand we can calculate: the average spin as a function of temperature and concentration by solving the appropriate system of mean field equations (Section 8.3.1); saturation moment per atom by solving for average spin at $T \approx 0K$ (8.3.2) and susceptibility by adding an external field to the mean one (8.4.1).

To calculate the hyperfine fields (Section 8.5), we need two other constants of proportionality, arrived at by fitting the average hyperfine field as a function of composition to experimental data. The theoretical average hyperfine field may be computed with knowledge of the

knowledge of the distribution of thermal average spins with respect to the identity of the first nearest neighbours. Since we are using a First Order model we have calculated only species-specific thermal averages but we may *decompose* this average into its class-specific components. In order to this we simply solve for the species averages and then substitute them into the mean fields for each class. The Brillouin functions are then evaluated. The result for a specific example is shown in fig.16.

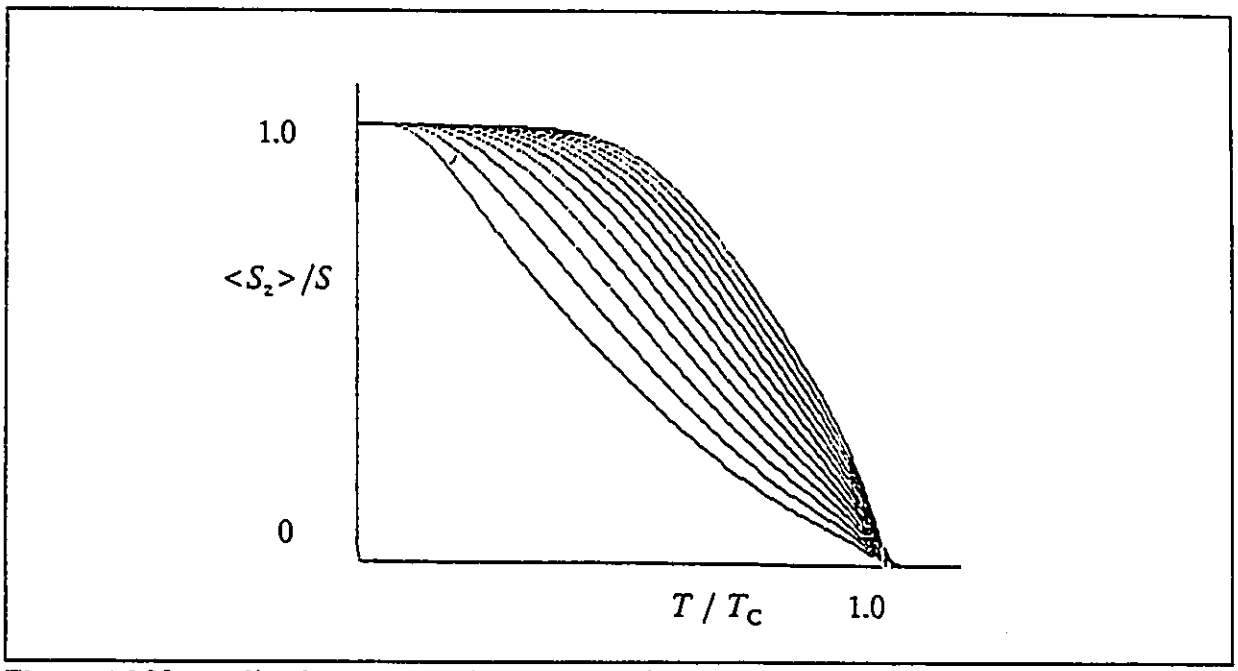


**Figure 16** Normalized average spin vs. temp. for species *A* decomposed into its 13 FOC components. ($z$ = 12, $S^A = S^B$ = 1, $J_{AA}$ = 20K, $J_{AB}$ = 40K, $J_{BB}$ = 60K)

This list by no means exhausts the type of calculation which can be performed. These properties have been chosen for their relevance to the real system we have studied, the fcc Fe-Ni alloys.

# 8/ FCC FE-NI ALLOYS - A TEST OF OUR MODEL

Our model has been applied (at the FO level) to the Fe-Ni alloys because (1) they are among the most complicated type of alloy systems, having mixed exchange and itinerant electrons and therefore pose a true challenge to a simple model and (2), due in part to interest in "Invar" they have been well-studied but are as yet not fully understood.

The nature and implications of itinerant electrons were discussed in Section 7.3; mixed exchange, Section 7.4. The fcc Fe-Ni alloys are known to be atomically random. The dominant exchange interactions of are the nearest neighbour ones. The general context in which the Fe-Ni alloys are of interest is discussed in Section 8.1.

Because an adequate explanation for even just the *magnetic* properties of Invar has not yet been proposed, we were motivated to find one. The entire alloy series comes under scrutiny as it is expected that the physical properties which lead to the distinctive invariance of one member must also exist in the others, just not expressed in the same way. The anomalous magnetic behaviour of these alloys is believed to be closely linked to the thermal anomalies.

## 8.1 OTHER MFT APPROACHES - FCC Fe-Ni

Other workers [4-15] have examined disordered alloys and related systems (amorphous alloys etc.) and several have attempted to develop a mean field method for such systems. We limit the discussion here to those which specifically address the fcc Fe-Ni alloys and employ three distinct exchange constants.

### 8.1.1 Müller and Hesse

The work of Müller and Hesse [12] is also based on a mixed exchange view of the alloys. They start from the assumption that of the three exchange parameters, only $J_{FeFe}$ is antiferromagnetic. Their approach to the problem of distribution of spin expectation values in the alloy is similar to ours in that they assume a discrete distribution of mean fields. However, in order to account for the proclivity of an Fe spin to align opposite its Fe neighbours, they modify the expression for the spatial/thermal average on Fe in the following manner. They consider an Fe atom with $n$ Fe neighbours to have any number from 0 to $n$ of these in an antiparallel position, but they take the probability of such occurrences to be given simply by:

$$P(n,c) = P(Fe\uparrow)^c \qquad (44)$$

where $c$ is the number of "up" Fe spins and where $P(Fe\uparrow)$ is the ratio of spin up Fe atoms. They admit that this is "valid for magnetically homogeneous binary alloys" while having stated in their introduction that "an inhomogeneous spin structure" is an "abnormal characteristic" of the Invar alloys.

Further, for a given $n$ they drop the actual distribution in favour of the *mean* configuration of up and down neighbours i.e. considering only those with $\overline{c}_n$ given by:

$$\overline{c}_n = \sum_{c=0}^{n} cP(n,c) . \qquad (45)$$

We have avoided the assumptions required by this device. In addition, they have imposed the condition that all Ni moments will be parallel. We have found this to emerge naturally given the physical properties of the system.

In order to determine the correct exchange constants, Müller and Hesse have taken the spin of Ni to be 0.5 and that of Fe to be 1.5 in order to approximate moments of $0.6\mu_B$ and $2.8\mu_B$ respectively. Recall that we have considered a distribution of moments in order to reach an effective spin value equal to that shown by experiment (Section 7.3). They have extracted the $J_{NiNi}$ value from the Curie point of pure Ni. With two free parameters $J_{FeNi}$ and $J_{FeFe}$ they have fit the total average spin of the system at $T = 0$[10] and $T = T_C$.

They have calculated the Curie point from the mean field equations. They interpret the concentration dependence of the Curie temperature to mean concentration dependence of the two constants $J_{FeFe}$ and $J_{FeNi}$. While their fit is good, it is least so in the range near 100 at% Ni even though they have used the corresponding Curie point to fix one of the three exchange parameters.

By allowing the exchange constants to vary with temperature they have achieved good success in reproducing the deviation of the saturation moment from the Slater–Pauling curve. We show

[10] Numerically, $T = 0$ is inaccessible so some low temperature, well below the transition point is used instead.

in Section 8.5.2 that this deviation emerges even when the exchange constants are fixed.

### 8.1.2 Menshikov

Also in the category of mixed exchange models is the work of Menshikov [13-15], who oversimplifies the nature of the inhomogeneity of the magnetic structure. Menshikov allows one mean field per species. The field is constructed as an average of the two extreme cases: nearest neighbours being all Ni or all Fe. This is a case of an Average Environment Model as discussed in Section 3.1.2. This is clearly less physical than either the model we present here or that of Müller and Hesse.

## 8.2 THE MAGNETIC PHASE DIAGRAM OF FE-NI

The Curie temperature is dependent on composition through probabilities. We have taken the theoretical curve for c(Ni) = 0 to 0.4 and compared it to experimental data [17]. We restrict our analysis to this regime where our model is most reliable, as discussed in Section 7.4.3. In addition the fcc Fe-Ni alloys are known to be perfect collinear ferromagnets for $c(Fe) < 40\text{at}\%$ [16]. By allowing the three exchange constants to vary freely we have minimized Chi−squared and determined the following values: $J_{FeFe} = (-20 \pm 10)\text{K}$, $J_{FeNi} = (280 \pm 10)\text{K}$ and $J_{NiNi} = (345 \pm 5)\text{K}$. We have estimated the uncertainty by varying the weighting given the experimental points and re-minimizing Chi-squared. The antiferromagnetic Fe-Fe interaction is consistent with the behaviour of the $\gamma$-phase of pure Fe [3].

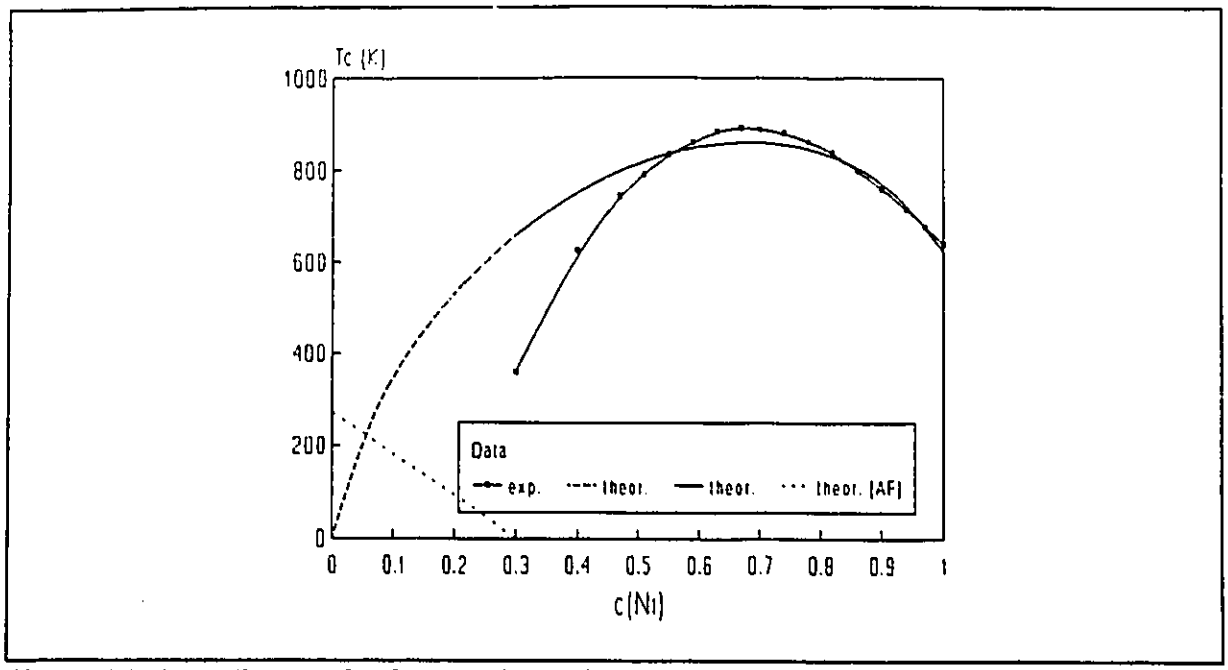


**Figure 17** Phase diagram for fcc Fe-Ni showing theoretical points (solid/dashed line represents $T_C$, dotted, $T_N$ as defined in Section 7.4) and experimental points (after Crangle and Hallan [7]).

It must be stressed that in the case of an fcc pure substance ferromagnet, the mean field Curie point found using *independently* obtained $J$'s[11] may be 25% higher than that actually observed [1]. This fact has not been taken into account here as the actual discrepancy for an alloy of our type is not known, nor will it be until a definitive method is developed. For this reason the exchange constants we use must be thought of as *effective* exchange constants.

The complete theoretical phase diagram obtained using Eq.(33) with the $J$'s given above is shown in fig.17 along with experimental points. The theoretical diagram covers all alloy concentrations, assuming an fcc lattice. In this figure the theoretical line is solid in the region in which its meaning is unambiguous in accordance with the interpretation of the effects of mixed exchange as discussed in Section 7.4. We find that our MFT approach predicts antiferromagnetic ordering for pure fcc Fe. However, pure fcc Fe might, in fact, be completely

[11] Spin-wave measurements using neutrons can give $J_{ij}$'s.

frustrated[12] and therefore have zero average spin at any temperature. This is not to be confused with actual antiferromagnetism in which the spatial average is zero despite non-zero averages on each site.

The real alloy series is believed to have a frustrated ferromagnetic nature with spin canting at high Fe concentrations up to the martensitic transition to the bcc phase. The existence of an antiferromagnetic phase for this system suggested by our phase diagram is a result of (1) the failure of MFT to incorporate the type of lattice in any meaningful way and (2) the failure of our MFT approach to allow canting explicitly.

## 8.3 AVERAGE SPIN AND THE SLATER-PAULING CURVE

### 8.3.1 Determining the Average Spin

Once the exchange parameters and spin quantum numbers are established, it is possible to calculate the magnetization curves at any concentration. For most compositions, the Brillouin function is of the expected form and solving the two coupled equations is achieved by iterating. This numerical method is described in Appendix II and a sample program appears in Appendix III. For high Fe concentrations the Brillouin functions are pathological and the mean field equations were solved by the more time-consuming method of bisection as discussed in Appendix II. The individual magnetization curves are of interest insofar as they demonstrate the expected flattening. The average spin calculations are also necessary for the purposes of determining the susceptibility and the hyperfine fields.

---

[12] The fcc lattice cannot be divided into interpenetrating sublattices with spin up atoms on one and spin down atoms on the other such that all antiferromagnetic bonds are satisfied.

### 8.3.2 The Slater-Pauling Curve

The Slater-Pauling curve is the expected intra-domain saturation moment at $T = 0$K as a function of alloy composition. It is a straight line representing the geometric combination of the atomic moments on each species computed as follows:

$$\langle \overline{S} \rangle_{SAT} = c(A)\, S^A + c(B)\, S^B. \qquad (46)$$

Mixed exchange ferromagnets deviate from this line in the regime in which the antiferromagnetic bonds are numerous. This is evidence for the existence of either canted spins (whose thermal averaged x and y components are randomly directed and therefore make their presence felt by diminishing the measured average moment) or *partial* or *latent antiferromagnetism* (where regions of collinear antiferromagnetic ordering occur).

In order to reproduce this result we solve for total average spin at 4.2K. We find (fig.18) a similar deviation at very nearly 60at% Ni. This is persuasive evidence that our model accounts for spin canting by depressing the average moment and an important result.

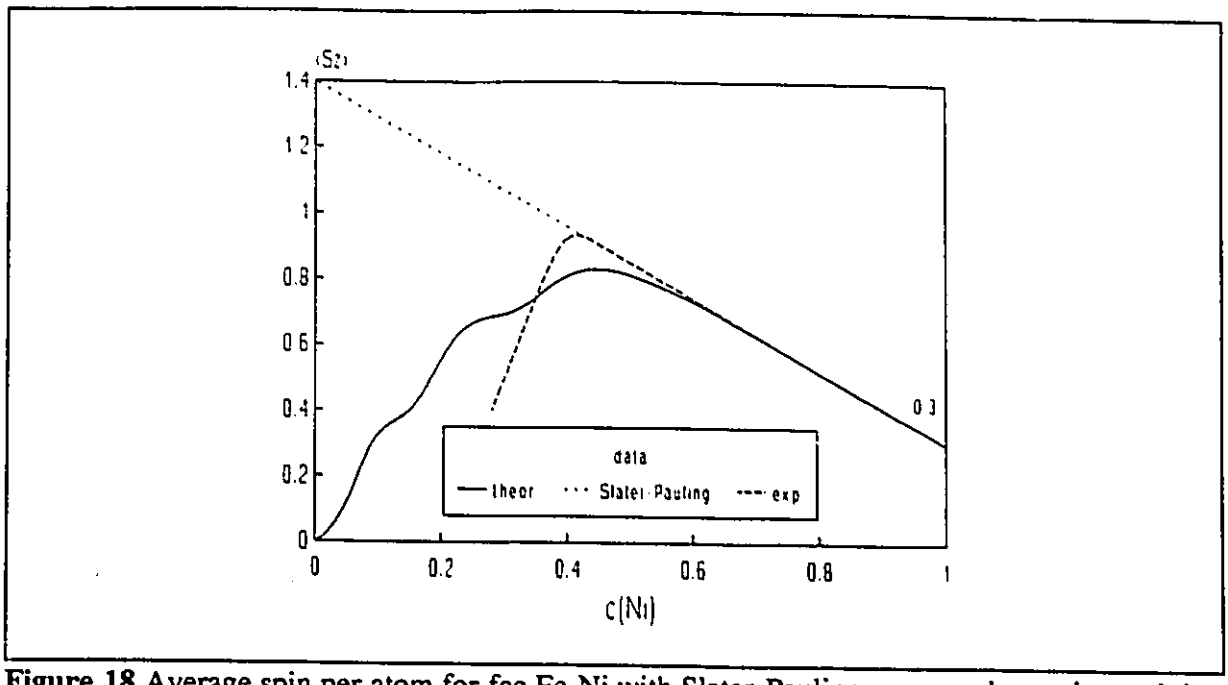


**Figure 18** Average spin per atom for fcc Fe-Ni with Slater-Pauling curve and experimental data [3].

## 8.4 THE EFFECT OF AN EXTERNAL FIELD : PARA-PROCESS SUSCEPTIBILITY

The behaviour of the Fe-rich members in an applied magnetic field provides an illustration of the effects of mixed exchange and a good test of our theoretical model. We determine the effect of a field on our theoretical system by adding a Zeeman term to the spin Hamiltonians. Susceptibility is a measure of the response of the system to an applied field and is defined as:

$$\chi \equiv \frac{\partial M}{\partial H}. \qquad (47)$$

As discussed earlier (Section 2.1.3), a ferromagnet in an applied field has its tendency toward parallel alignment of moments reinforced. Therefore, by applying a magnetic field we may expect a larger average spin than that which arises spontaneously at the same temperature. We have established that in the case of a system which contains some antiferromagnetic bonds, and in the absence of a field, some spins may assume positions which are antiparallel or canted with respect to the +z direction. These spins, when subject to an external field, may be coerced into parallel alignment, a phenomenon known as *para-process susceptibility*.

The average spin shows a near-linear increase with field at low temperatures and high fields in which normal ferromagnets are saturated [3]. The higher the Fe concentration the higher this susceptibility (as shown in fig.19), implying an increase in the number of spins which are not aligned.

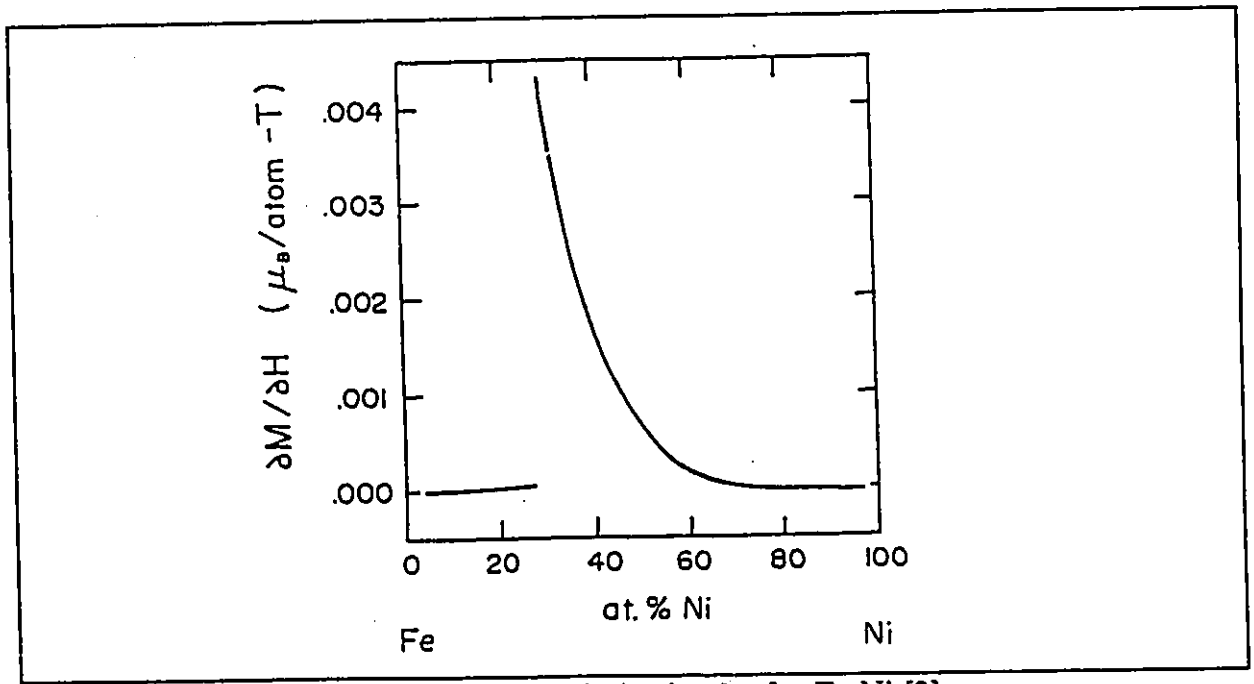


**Figure 19a** Measured para-process field derivative for fcc Fe-Ni [3].

in fig.19b for three concentrations of Fe) due to the discrete distribution of sites which we have adopted. A step occurs when an entire class of canted spins is forced into parallel alignment. As expected, we see the average slope of the lines becoming higher at higher Fe concentrations.

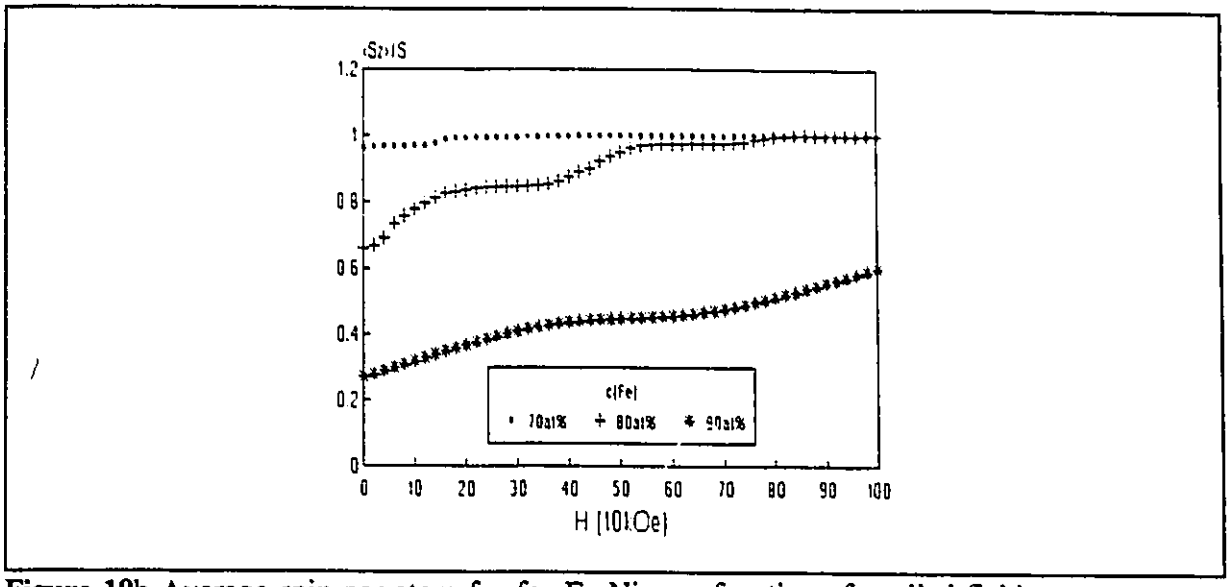


**Figure 19b** Average spin per atom for fcc Fe-Ni as a function of applied field.

## 8.5 HYPERFINE FIELD CALCULATIONS

### 8.5.1 Description

The nucleus of an Fe-57 atom is immersed in a magnetic field known as the *hyperfine field* which splits the nuclear energy levels, an effect which may be detected by Mössbauer spectroscopy. A new method [16,18] makes it possible to extract the distribution of hyperfine fields among the sites of the alloy. The hyperfine field is a function of the moments on the atom itself and on its nearest neighbours, thus we are able to calculate it from our mean field results.

### 8.5.2 Theoretical Calculation of the Average Hyperfine Field

In order to find the theoretical distribution of hyperfine fields we begin by considering the field on an Fe atom which has $n$ Fe nearest neighbours, at a temperature $T$:

$$H_{T,n}^{hff} = H_l^n + H_t^n \tag{48}$$

where $H_l^n$ is the *local* term and $H_t^n$ is the *transferred* term. These fields are related to the moments via [16]:

$$\begin{aligned} H_l^n &= a\langle S_z^{Fe,n}\rangle \\ H_t^n &= b\left(n\langle \overline{S}_z^{Fe}\rangle + (12-n)\langle \overline{S}_z^{Ni}\rangle\right) \end{aligned} \tag{49}$$

where $a$ and $b$ are constants of proportionality which deliver fields in the correct units. The averages required for the local term are derived by the decomposition method of Section 7.5.

Once we have determined the hyperfine fields for $n = 0$ to 12, we can combine these to get the average hyperfine field thus:

$$\overline{H}_T^{hff} = \sum_{n=0}^{12} P(12,n)\, H_{T,n}^{hff} \tag{50}$$

at any temperature and concentration of Fe.

### 8.5.3 Fitting to Obtain Parameters

It has been shown [16] that the experimentally measured average hyperfine field may be described by a linear function of concentration for room and liquid nitrogen temperatures and at concentrations of Fe $<$ 45at%. We fit the calculated average hyperfine field as a function of Fe concentration to the experimental data in the relevant concentration range with $a$ and $b$ as fitting parameters. We also use data collected at liquid He temperature and c(Fe) $\approx$ 0 [19] for the purposes of fitting. We extrapolated a slope for the liquid helium average hyperfine field vs. concentration function from those at the higher temperatures.

We fit at all three temperatures simultaneously after failing to find constants from individual temperature fits which agreed amongst themselves. The weighting given the data was in the ratio 10:5:1 for liquid helium, liquid nitrogen and room temperatures. We found a minimum of Chi−squared at $a$ = 170kOe and $b$ = 12kOe. The fit is illustrated in Appendix VI.

### 8.5.4 Comparison of Average Hyperfine Field Results

With values for $a$ and $b$ we can calculate the average hyperfine field at liquid nitrogen temperature for the entire alloy series as shown in fig.20. The theoretical average field has linear concentration dependence up to about 60at%Fe. The experimental result is linear up to 55at%Fe at this temperature. This lack of agreement can be attributed to the overestimation of average spins by our model. This overestimation occurs throughout the ferromagnetic regime. It is an artifact of the FO model which, as pointed out in Chapter 6, shows less average spin depression than do the higher order models.

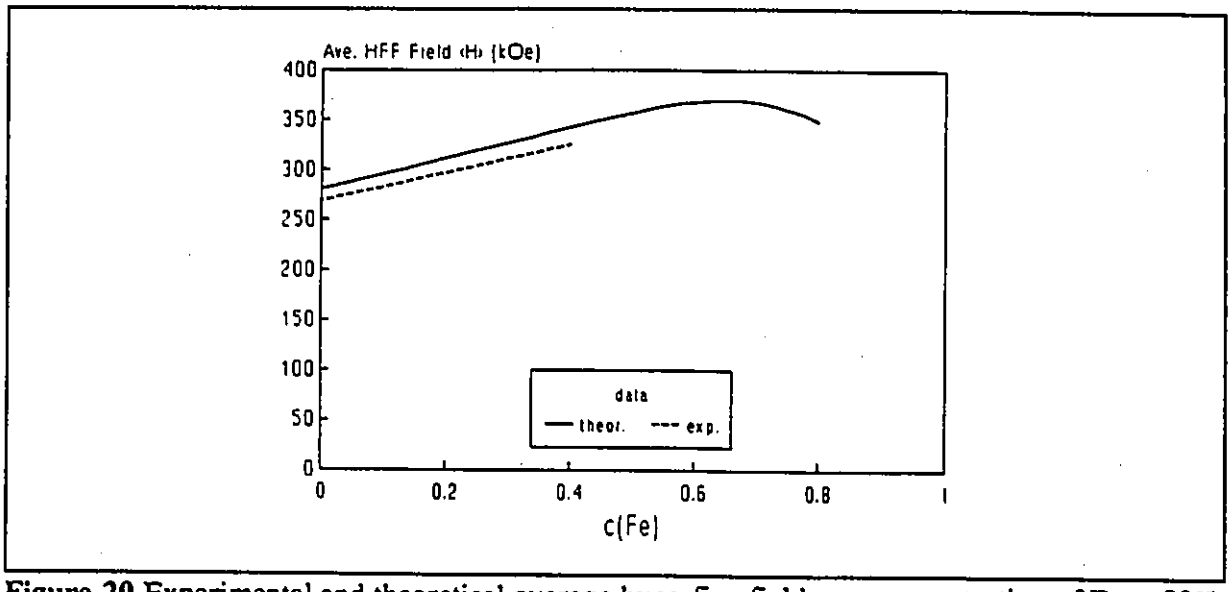


**Figure 20** Experimental and theoretical average hyperfine fields vs. concentration of Fe at 80K.

Since it is expected that these constants are not temperature sensitive we blame this discrepancy on the failure of our model to provide perfect results for the average moment carried by each species. The qualitative trend is correct, however. We see a linear dependence on Fe concentration, however we overestimate the intercept and the slope of the line at both liquid nitrogen and room temperature (not shown).

### 8.5.5 Hyperfine Field Distributions

Upon comparing the theoretical distribution with that extracted from experimental data [20] (figs.21a through 21d) we find good agreement, particularly at the lowest Fe concentrations. (Note that the lines drawn in these figures are included for emphasis only.) The discrepancy is the result of the choice of $a$ and $b$. Otherwise, the qualitative agreement supports our view of the fcc Fe-Ni alloys.

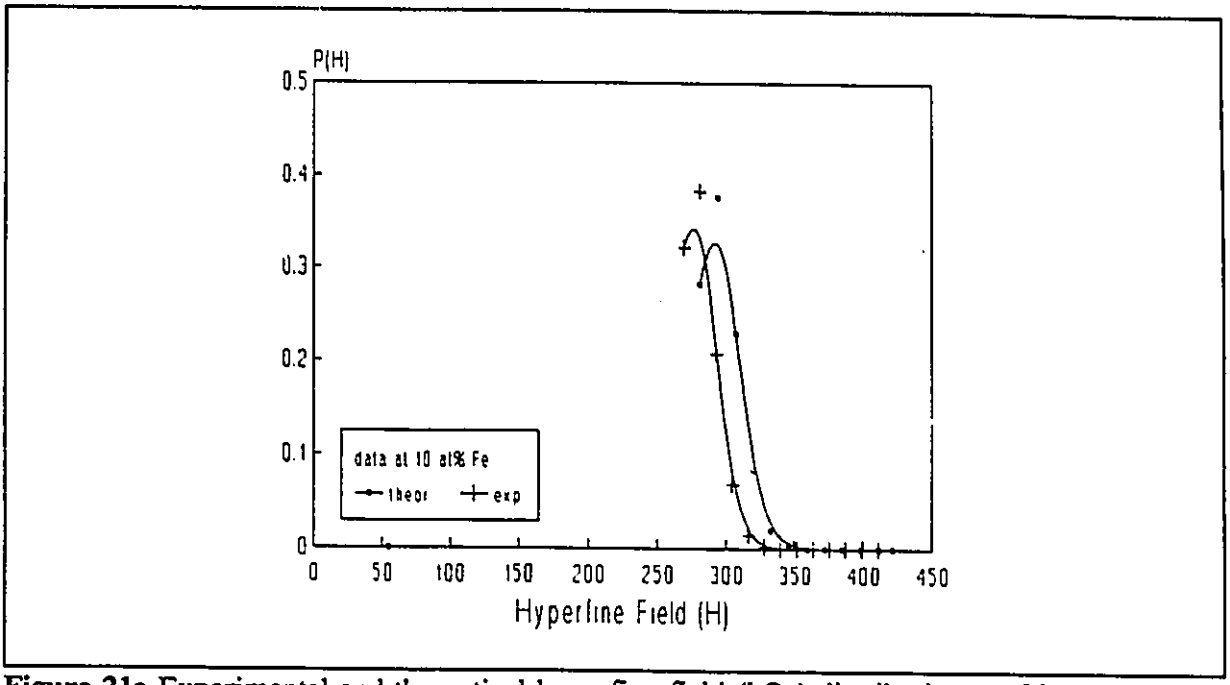


**Figure 21a** Experimental and theoretical hyperfine field (kOe) distributions at 80K and 10 at% Fe.

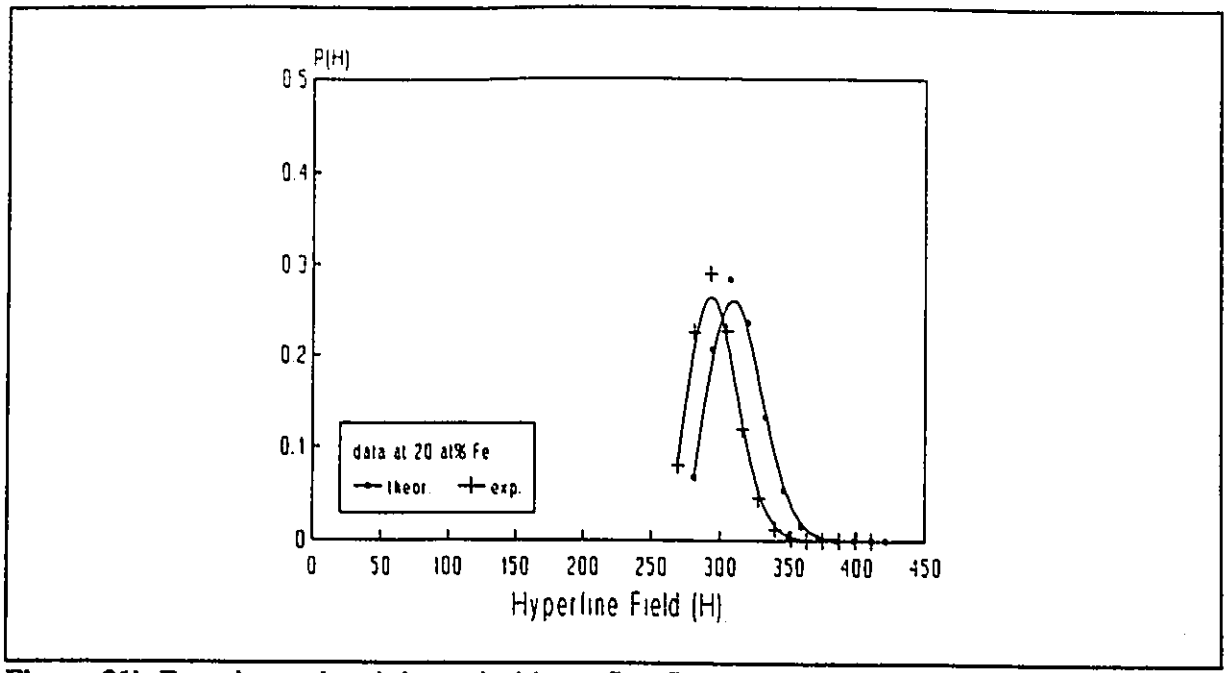


**Figure 21b** Experimental and theoretical hyperfine field (kOe) distributions at 80K and 20 at% Fe.

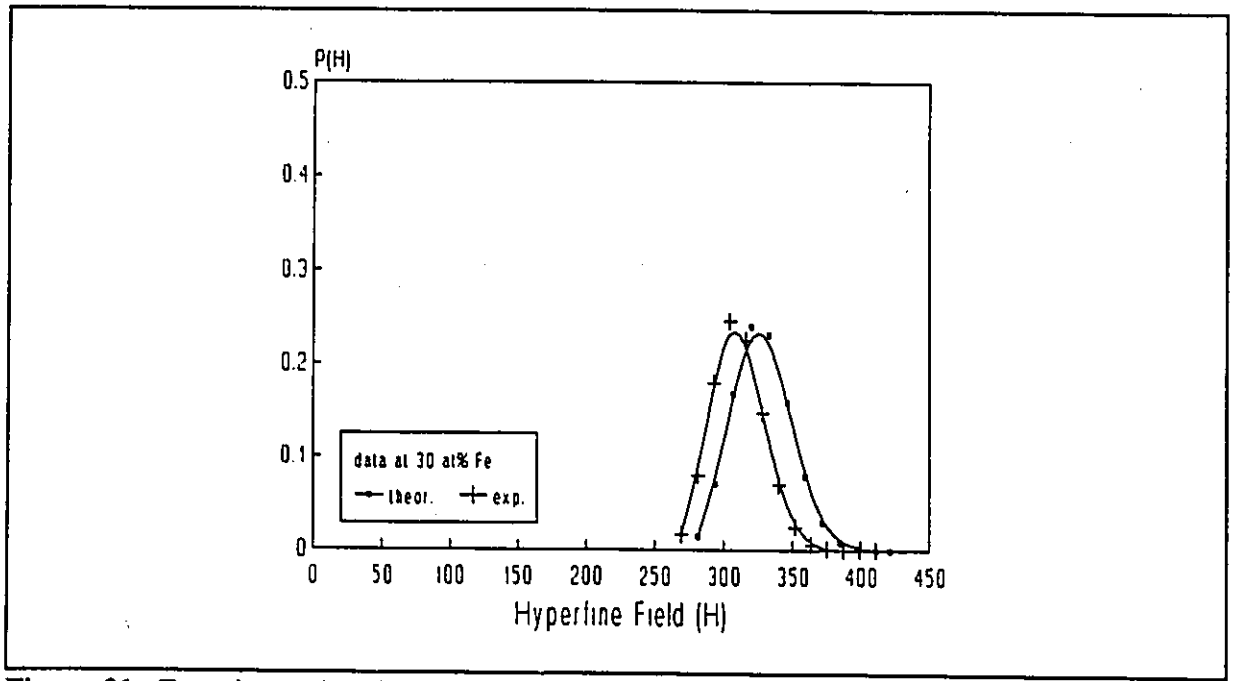


**Figure 21c** Experimental and theoretical hyperfine field (kOe) distributions at 80K and 30 at% Fe.

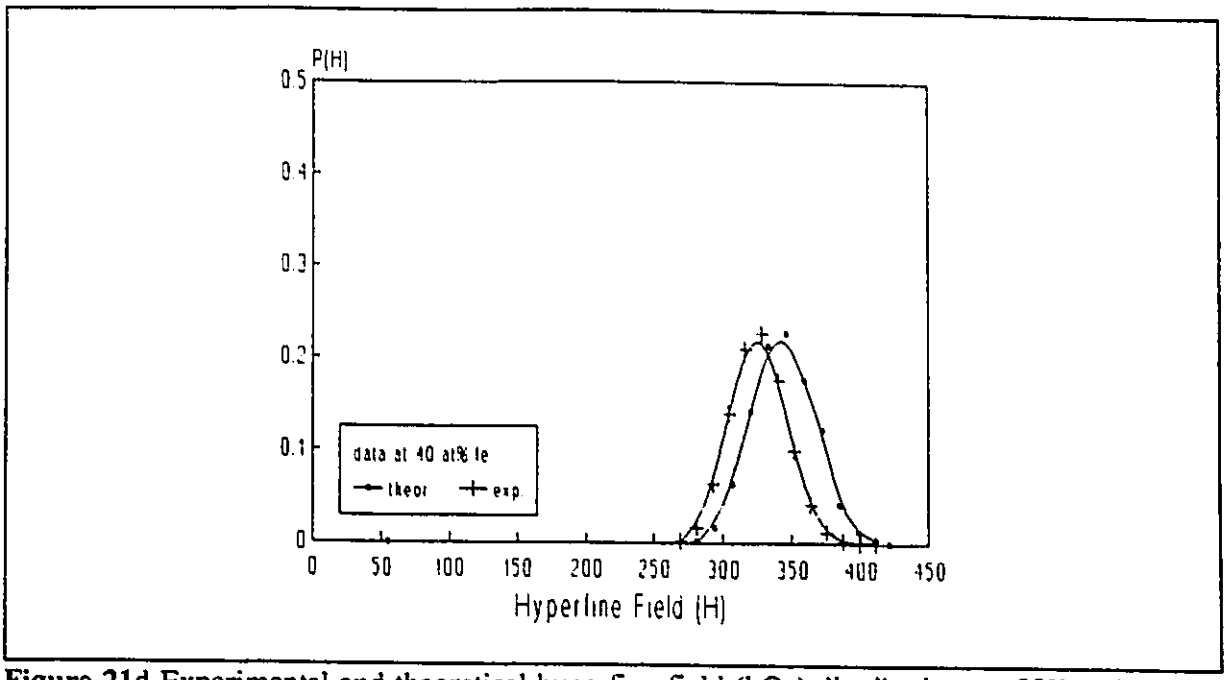


**Figure 21d** Experimental and theoretical hyperfine field (kOe) distributions at 80K and 40 at% Fe.

## 8.6 SUMMARY

The results for our comparison with the real Fe-Ni alloy series show significant qualitative agreement for the phase diagram (fig.17), high field susceptibility (fig.19b), deviation from the Slater-Pauling curve (fig.18), average hyperfine field (fig.20), and hyperfine field distributions (figs.21a through 21d). Discrepancies may largely be attributed to the tendency of our FO model to overestimate average spins.

# 9/ CONCLUSION

The conclusions we can draw from this work are (1) that flattened magnetization curves are the result of randomness, (2) that the model is, in principle, sound and, in the limit of many classes should deliver the correct mean field solution for a ferromagnetic alloy, (3) that our treatment of itinerant electrons is reasonable but that (4) the model (at the FO level) falls short of quantitative success in the most complicated case to which it could be applied: namely a 3-D random alloy having itinerant electrons and mixed exchange.

The convergence of the results of the Second and Third Order Models shown in Chapter 5 is evidence that our approach of classifying spins and thereby substituting a discrete distribution for the real continuous one is appropriate and productive.

Chapter 6 compared two systems which only differed in that one had atoms arranged randomly while the other was atomically ordered. The only difference in the resulting magnetization curves is that the one for the random alloy is flattened, thus we are able to conclude that this is an effect of randomness.

The test of our model with a real 3-D system demonstrates that our First Order model is, in the case of a metallic mixed exchange alloy, a good first approximation. *For the first time*, the main anomalous characteristics of the magnetic behaviour are predicted without having recourse to temperature-dependent exchange constants or spin magnitudes, while allowing a (discrete) distribution of site-specific thermally averaged moments as exists in the real material. Indeed, our FO model does generate qualitatively correct distributions in agreement with hyperfine field

distributions from Mössbauer spectroscopy.

Some features of our calculations (such as the stepwise field dependence in fig.19b) are the result of using a discrete distribution over classes. This type of artifact can be expected to disappear in the limit of many classes.

Other discrepancies with experimental data are also the result of using too few classes; averaging over FOs masks a great deal of detail. By necessity, we have included in one sum terms which, because of the identity of the nearest neighbours and the presence of both types of interactions, may be very different, as shown by the decomposition of such a sum into its parts in fig.16. This is analogous to the case of an antiferromagnet, wherein describing the average spin as *zero* is legitimate although it disguises the fact that there are sublattices which in themselves may show perfect spin ordering. We expect that if a higher order class model could be applied to this real system that there would be a significant improvement in results and, eventually, convergence as in the case of the 1-D alloy.

Investigations in the realm of the thermal and elastic properties of random alloys as predicted by our mean field approach is a logical next step, particularly with a view to the anomalous Invar behaviour.

## APPENDIX I SYMBOLS AND ABBREVIATIONS

In order of appearance:

fcc face-centred cubic
$N$ number of atoms/sites in system
$F_i$ value of local property on $i^{th}$ atom/site
$P(k)$ probability of finding a site in class $k$
$H_i$ Hamiltonian for $i^{th}$ atom/site
$J_{ij}$ exchange constant for interaction between spins $i$ and $j$
$\vec{S}$ spin angular momentum
z coordination number of lattice = no. of nn's
nn nearest neighbour
$\vec{\mu}$ magnetic moment
g Landé g-factor
$\mu_B$ Bohr magneton
$\vec{H}$ external field
$H_Z$ Zeeman Hamiltonian
$S$ spin quantum number
$\langle S_z^i \rangle$ thermal average z component of $i^{th}$spin
$\beta$ $1/k_BT$
$k_B$ Boltzmann constant
$T$ temperature in Kelvin
$Z$ partition function
$\langle \vec{S} \rangle$ spatial/thermal average z component of spin
$H_m$ mean field Hamiltonian
$\lambda$ mean field coefficient
$S_z^i$ z component of $i^{th}$ spin
$B_S$ Brillouin function
$T_C$ Curie temperature, transition temperature for ferromagnets
$S^A$ spin quantum number for species/sublattice $A$
AI Average Interaction
$J_{AB}$ exchange constant for $A$-$B$ interaction
$P(AB)$ probability for $A$-$B$ interaction
$c(A)$ concentration of species $A$
$AE$ Average Environment
$\overline{H}_A$ mean field for a spin of species/sublattice $A$
ZOC Zeroth Order Class
FOC First Order Class
$A,n$ FOC for species $A$-type with $n$ $A$-type nn's
$n$ number of $A$-type atoms in first coord. shell
$P(z,n)$ probability of $n$ $A$-type nn's out of $z$

$P(A,z,n)$ probability of $A$-type atom having $n$ $A$-type nn's out of z

$\overline{H}_{A,n}$ mean field for FOC $A,n$

$\langle S_z^{A,n} \rangle$ thermal average for FOC $A,n$

$\langle \overline{S}_z^{A} \rangle$ spatial/thermal average for spins of species $A$

$\langle \overline{S}_z \rangle$ spatial/thermal average spin per atom

SOC Second Order Class

$\overline{H}_{A,n,m}$ mean field for spin of SOC $A,n,m$

$\langle S_z^{A,n,m} \rangle$ thermal average for spin of SOC $A,n,m$

$\langle \overline{S}_z^{A,n} \rangle$ spatial/thermal average spin for atoms of FOC $A,n$

TOC Third Order Class

$T_N$ Néel temperature, for antiferromagnets

$P(n,c)$ probability of an Fe atom having $c$ up Fe nn's out of $n$

$P(Fe\uparrow)$ ratio of spin up Fe atoms to all Fe atoms

$\overline{c}$ average no. of spin up Fe's

$\overline{H}_T^{hff}$ average hyperfine field at temp. T

$H_n$ hyperfine field for Fe atom with $n$ Fe nearest neighbours

$H_l$ local component of hyperfine field

$H_t$ transferred component of hyperfine field

$a$ constant for local component of hyperfine field

$b$ constant for transferred component of hyperfine field

## APPENDIX II Technical Notes - Numerical Methods

The solution of simultaneous non-linear equations was the chief technical challenge encountered in this project. The equations in question are sums of Brillouin functions. In the case of the First Order Model, in which there are two equations in two unknowns, the system of equations may be represented by:

$$x = X(x,y) \quad (1)$$

$$y = Y(x,y) \quad (2)$$

which are generally solvable by estimating the solution $(x_0,y_0)$ and then iterating until an $(x,y)$ is found that differs from the previous generation by less than 1.E-12. The (normalized) functions $X$ and $Y$ are bounded by (+1,-1). In general for any $y$ there is a solution for Eq.(1) and for any $x$ there is a solution for Eq.(2). Therefore, in practice, we solve Eq.(1) for our initial guess at $y$ $(y_0)$, yielding a new estimate of $x$. By "solve" we mean finding an $x$ which satisfies the equation or, more specifically, an $x_n$ which agrees with the previous generation $x_{n-1}$ by less 1E-12. If this condition is not met within a preset number of iterations the procedure stops and the value of $x$ at that time is taken to be the updated value. This procedure constitutes a *minor iteration loop*. The new estimate of $x$ is then used to solve Eq.(2) to arrive at a new estimate of $y$. This entire procedure constitutes a *major iteration loop*. An example of this type of program appears in Appendix III. The algorithm is outlined below:

```
set x0,y0
x = x0
y = y0
for j = 1 to nj
  for i = 1 to ni
    nx = X(x,y)
    if abs(nx - x) is less than 1.E-12 then
      go to 10
    else
      x = nx
    end if
  next i
```

```
10   x = nx
       for i = 1 to n1
         ny = Y(x,y)
         if abs(ny - y) is less than 1.E-12 then
           go to 20
         else
           y = ny
         end if
       next i
20   y = ny
     next j
```

This is not the only way of proceeding. Alternatively we can evaluate each function only once during the major iteration loop. Both of these methods were tested and found to be viable and similar in efficiency. The choice of the first method was one of preference and ease in algorithm construction when higher order models were considered.

The solutions found were always tested to verify that they satisfied each equation and in addition that they were reasonable given the parameters involved, i.e. the solution reflected a ferromagnetic state for a system whose exchange constants favoured ferromagnetic ordering.

Because we (1) know the form of these functions and (2) expect a solution in the range (+1,-1) (we are seeking normalized average spin), we are able to begin the iteration process with a very good initial guess. For example, for a system in which all $J$'s are positive the initial guess (1,1) will always lead to a solution, usually in something like 100 major iterations comprising 10 to 20 minor iterations for each function for a tolerance of 1.E-12.

The same procedure may be followed with the higher order models which have more equations. In these higher order models, solving the system of equations is simplified because most

equations do not depend on all the variables. For the Second Order Model there are six equations in six unknowns:

$$A0 = A0(B0, B1) \qquad (1)$$

$$A1 = A1(A1, A2, B0, B1) \qquad (2)$$

$$A2 = A2(A1, A2) \qquad (3)$$

$$B0 = B0(A0, A1) \qquad (4)$$

$$B1 = B1(A0, A1, B1, B2) \qquad (5)$$

$$B2 = B2(B1, B2) \qquad (6)$$

The functions have at most four variables and in fact Eqs.(1) and (4) are not of the type $x = X(x,\ldots)$ at all. The implications of this are that these two equations need not be iterated on and our solution need not "satisfy" these equations in the same way as it must satisfy the other four. Our problem is much more like solving four equations in four unknowns. The algorithm is outlined below:

set $A0_0, A1_0, A2_0, B0_0, B1_0, B2_0$
$A0 = A0_0$
$A1 = A1_0$
$A2 = A2_0$
$B0 = B0_0$
$B1 = B1_0$
$B2 = B2_0$

for j = 1 to nj

  $A0 = A0(B0,B1)$

 for i = 1 to n1
  $nA1 = A1(A1,A2,B0,B1)$
  if abs($nA1$ - $A1$) is less than 1.E-12 then
   go to 20
  else
   $A1 = nA1$
  end if
 next i

20 $A1 = nA1$

 for i = 1 to ni
  $nA2 = A2(A1,A2)$

```
      if abs(nA2 - A2) is less than 1.E-12 then
    go to 30
      else
        A2 = nA2
      end if
    next i

30  A2 = nA2

    B0 = B0(A1,A2)

    for i = 1 to ni
      nB1 = B1(A0,A1,B1,B2)
      if abs(nB1 - B1) is less than 1.E-12 then
        go to 50
      else
        B1 = nB1
      end if
    next i

50  B1 = nB1

    for i = 1 to n1
      nB2 = B2(B1,B2)
      if abs(nB2 - B2) is less than 1.E-12 then
        go to 60
      else
        B2 = nB2
      end if
    next i

60  B2 = nB2

  next j
```

Again, we know that the solution for each variable lies between +1 and -1 and we are able to make an intelligent first guess at the solution.

For the Third Order Model the algorithm is an extension of the those shown above.

As was discussed in Section 7.4, Brillouin functions for Fe spins at high Fe concentrations are often pathological and the iteration method fails. In general, the Brillouin functions for Ni are

normal regardless of temperature and concentration. In such cases, iteration provides a "pseudo-solution" or a solution to $x = -X(x,y)$.

In order to find the "true" solution, that one pertaining to $x = X(x,y)$, the method of bisection was used to find the root of $X(x,y) - x = 0$. This method entails bracketing the root between $x_U$ and $x_L$ and then evaluating the function $X$ at these points and also at a point $x_B$ midway between them. The sign of the function at $x_B$ is compared with the sign $X(x_U,y)$; if it is the same then $x_B$ becomes the new $x_U$. If the signs are not the same then $x_B$ becomes the new $x_L$. A *new* midway point is then defined and the process repeated. In this way the test point always comes closer to the root. A tolerance is defined at which the difference between the upper and lower brackets is considered to be negligible; at this point a solution is assumed. The success of this method depends on the possibility of finding a solution to $y = Y(x,y)$ for any $y$.

Other calculations were straightforward. Most programs solved the system of equations under varying conditions of temperature, concentration or external field. All programs (a final number of about twenty useful ones) were written in *Turbo Basic*.

## APPENDIX III SAMPLE PROGRAM

```
'CONALG2S.BAS
'This program calculates the magnetization of a disordered
'binary alloy ferromagnet with three exchange integrals and
'any number of nearest neighbours using mean field theory
'and writes it to CAA.DAT,CAB.DAT,CAM.DAT
'It uses the conventional (iteration) algorithm and warms through Tc.
'It allows for two non-half integer spin species.
'
'
screen 2:cls
OPEN "B:CAA.DAT" FOR OUTPUT AS #1 LEN=20000
OPEN "B:CAB.DAT" FOR OUTPUT AS #2 LEN=20000
OPEN "B:CAM.DAT" FOR OUTPUT AS #3 LEN=20000
OPEN "A:CA.DAT" FOR OUTPUT AS #4 LEN=20000
OPEN "B:check2.DAT" FOR OUTPUT AS #7 LEN=20000
DIM MAGN#(1000)
DIM MAGNA#(1000)
DIM MAGNB#(1000)
DIM PROB#(100)

'SET PARAMETERS FOR ALGORITHM
size = 100
TK# = 8.
INPUT "Enter the number of major iterations       : ", NIT#
INPUT "Enter the number of minor iterations       : ", NITT#
INPUT "Enter the number of temperatures           : ", NT#

'SET PARAMETERS FOR SPIN SPECIES A (Ni)
INPUT "For species A (Ni) enter SAU#              : ", SAU#
NMSAU = INT(2*SAU# + 1)
INPUT "For species A (Ni) enter SAL#              : ", SAL#
NMSAL = INT(2*SAL# + 1)
INPUT "For species A (Ni) enter alpha             : ", ALPH#
SA# = ALPH# * SAU# + (1 - ALPH#) * SAL#

'SET PARAMETERS FOR SPIN SPECIES B (Fe)
INPUT "For species B (Fe) enter SBU#              : ", SBU#
NMSBU = INT(2*SBU# + 1)
INPUT "For species B (Fe) enter SBL#              : ", SBL#
NMSBL = INT(2*SBL# + 1)
INPUT "For species B (Fe) enter beta              : ", BET#
SB# = BET# * SBU# + (1 - BET#) * SBL#

INPUT "Enter the number of near neighbours NNN    : ", NNN#
INPUT "Enter the nn exchange JAA in degrees Kelvin: ", JAA#
INPUT "Enter the nn exchange JAB in degrees Kelvin: ", JAB#
INPUT "Enter the nn exchange JBB in degrees Kelvin: ", JBB#
INPUT "Enter the concentration CA# of A-type atoms: ", CA#
SAVA# = SA#
SAVB# = SB#
CB# = 1 - CA#
```

```
'CALC. PROBS. FOR GIVEN CA#
CALL PTABLE(PROBA#(),PROBB#(),size)

'CALCULATE THE THEORETICAL TRANSITION TEMPERATURES
AL# = 0
BE# = 0

FOR NC% = 0 TO NNN#
  AL# =  AL# + NC% * PROBA#(NC%)
  BE# =  BE# + NC% * PROBB#(NC%)
NEXT NC%
AL1# = AL# * SA# * (SA# + 1) * JAA# / 3
AL2# = AL1# * JAB# / JAA#
BE1# = BE# * SB# * (SB# + 1) * JBB# / 3
BE2# = BE1# * JAB# / JBB#
QA# = 1
QB# = -1 * (AL1# + BE1#)
QC# = AL1# * BE1# - AL2# * BE2#
TC1# = (-1 * QB# + SQR(QB#^2 - 4 * QC#)) / 2
TC2# = (-1 * QB# - SQR(QB#^2 - 4 * QC#)) / 2
PRINT "TC1#, TC2# = ",TC1#,TC2#

'APPLY CONVENTIONAL ALGORITHM
FOR T% = 1 TO NT#
  PRINT "temperature step counter :",T%
  TK# = TK# + 2.

  FOR IT% = 1 TO NIT#
    A# = SAVA#

    'FIND B# FOR THIS A# BY SOLVING B# = g(B#) BY CON. ALG.
    FOR ITT% = 1 TO NITT#
      B# = SAVB#
      CALL CALCM(A#,B#,SBU#,NMSBU,JBB#,JAB#,PROBB#(),size)
      SAVB# = M#
      CALL CALCM(A#,B#,SBL#,NMSBL,JBB#,JAB#,PROBB#(),size)
      SAVB# = BET# * SAVB# + (1 - BET#) * M#
      IF abs(B# - SAVB#) < 1.E-12 THEN GOTO 21
    NEXT ITT%

21  B# = SAVB#

    'FIND f(A#) = ALPH# * f(AU#) + (1 - ALPH#) * f(AL#)
    CALL CALCM(B#,A#,SAU#,NMSAU,JAA#,JAB#,PROBA#(),size)
    SAVA# = M#
    CALL CALCM(B#,A#,SAL#,NMSAL,JAA#,JAB#,PROBA#(),size)
    SAVA# = ALPH# * SAVA# + (1 - ALPH#) * M#

  NEXT IT%

  MAGNA#(T%) = SAVA#
  MAGNB#(T%) = SAVB#
  MAGN#(T%) = CA#*MAGNA#(T%) + CB#*MAGNB#(T%)

NEXT T%
```

```
'SUBROUTINE TO CALC. THE PROBABILITIES OF THE VARIOUS SUBLATTICES GIVEN CA#
SUB PTABLE(PRBLTA#(1),PRBLTB#(1),size)
    SHARED NNN#,CA#,CB#
    LOCAL NA#,NB#

    PI# = FNFACT#(NNN#)
    NA# = 0.
    NB# = NNN#
    IN% = NNN#
    FOR IND% = 0 TO NNN#
      P# = PI# * (CA#)^NA# * (CB#)^NB#
      PRBLTA#(IND%) = P# / (FNFACT#(NA#)*FNFACT#(NB#))
      PRBLTB#(IN%) = PRBLTA#(IND%)
      NA# = NA# + 1.
      NB# = NB# - 1.
      IN% = IN% - 1
    NEXT IND%

END SUB

DEF FNFACT#(X#)
    LOCAL I%,TOTAL#

    IF X# < 0. OR X# > 170. THEN FNFACT# = -1 : EXIT DEF
    TOTAL# = 1
    FOR I% = X# TO 2 STEP -1
      TOTAL# = TOTAL# * I%
    NEXT I%
    FNFACT# = TOTAL#
END DEF

98      'SUBROUTINE TO TRANSFORM TO SCREEN COORDINATES
        XP = MH * X + BH
        YP = MV * Y + BV
```

```
'SUBROUTINE TO CALCULATE f(A#) OR g(B#)
SUB CALCM(F#,V#,S#,NMS,JV#,JF#,PROB#(1),size)
    SHARED M#,TK#,NNN#
    DIM SUM#(100)
    DIM ZZ#(100)
    DIM DD#(100)
    DIM MSL#(100)
    M# = 0.
    'IF JF#  0.0 THEN F# = -1 * F#

    'INITIALIZE VARIABLE TO ZERO
    FOR IND% = 0 to NNN#
      SUM#(IND%) = 0.
      ZZ#(IND%) = 0.
    NEXT IND%

    'SUM OVER POSSIBLE ORIENTATIONS OF THE CENTRAL SPIN (Sz)
    FOR MS% = 1 to NMS
      NF# = NNN#
      NV# = 0.

      'RUN OVER THE POSSIBLE SUBLATTICES FOR THIS S# = Sz
      FOR IND% = 0 TO NNN#
        DD#(IND%) = -(NF#*S#*JF#*F# + NV#*S#*JV#*V#) / TK#
        SUM#(IND%) = SUM#(IND%) + S# * EXP(-DD#(IND%))
        ZZ#(IND%) = ZZ#(IND%) + EXP(-DD#(IND%))
        NF# = NF# - 1.
        NV# = NV# + 1.
      NEXT IND%

      S# = S# - 1
    NEXT MS%

    S# = S# + NMS
    M# = 0.

    'OBTAIN A# BY SUMMING OVER Ai#'S (SUBLATTICES)
    FOR IND% = 0 TO NNN#
      MSL#(IND%) = SUM#(IND%) / (ZZ#(IND%))
      M# = M# + PROB#(IND%)* MSL#(IND%)
    NEXT IND%

END SUB
```

```
'SET UP SCREEN
CLS
PSET(0,0):PSET(639,0):PSET(639,199):PSET(0,199)
pset(319,0):pset(319,199)

'DETERMINE SCALING FACTORS FOR PLOT
YMAX = SA#
IF SB# > SA# THEN YMAX = SB#
YMIN = -1 * YMAX
XMIN = 8.
XMAX = XMIN + 2. * NT#
MH = 639./ (XMAX - XMIN)
BH = -MH * XMIN
MV = 199. / (YMIN - YMAX)
BV = -MV * YMAX

'SET STARTING POSITION
X = XMIN
Y = YMAX
GOSUB 98
PSET (XP,YP)

'PLOT NORMALIZED SPONTANEOUS MAGNETIZATION VERSUS TEMPERATURE FOR TYPE A
FOR J% = 1 TO NT#
X = X + 2.
Y = MAGNA#(J%) / YMAX
GOSUB 98
LINE -(XP,YP), 1
WRITE #4,X,MAGNA#(J%),MAGNB#(J%),MAGN#(J%)
NEXT J%

CLOSE #1
CLOSE #2
CLOSE #3
CLOSE #4
CLOSE #7
END
```

## APPENDIX IV SUBLATTICE TREATMENT OF A PURE ANTIFERROMAGNET

In a pure antiferromagnet the exchange interaction promotes antiparallel alignment of neighbouring spins. In many lattices this can be accommodated without frustration, notable exceptions being the 2-D triangular lattice and the 3-D fcc lattice. A pure antiferromagnet comprises two (or more) interpenetrating sublattices, one with spins predominantly "up" and the other with spins predominantly "down".

The sublattices of a typical 2-D square antiferromagnet may be visualized as follows:

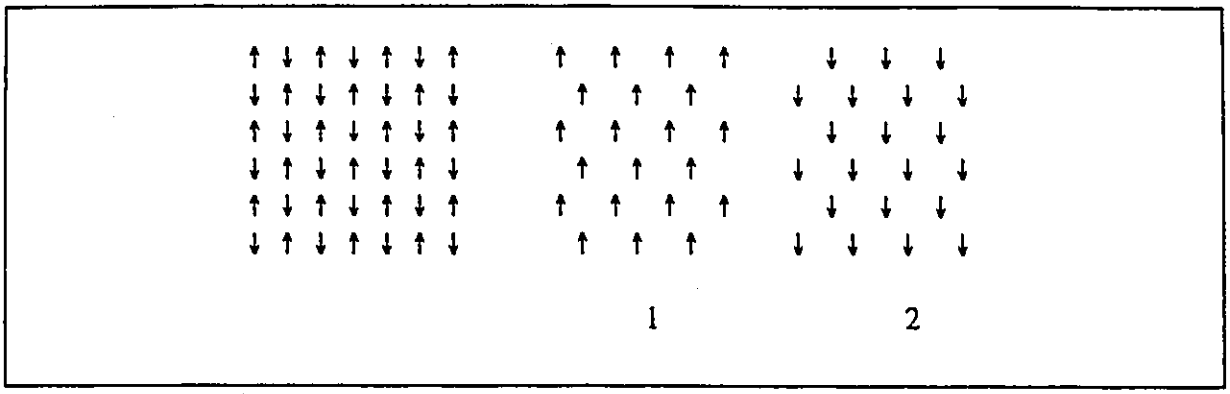


**Figure A1** Sublattices of a 2-D square antiferromagnet.

The analysis follows that of the ferrimagnet (Section 2.4); we find that the thermal average for spins on one sublattice (labelled 1) depends on the average spin on the other sublattice (labelled 2). We find two equations in two unknowns:

$$\langle S_z^1 \rangle = SB_S(-\beta |J| zS \langle S_z^2 \rangle) \qquad \text{A1}$$

$$\langle S_z^2 \rangle = SB_S(-\beta |J| zS \langle S_z^1 \rangle)$$

These coupled equations may be solved numerically at any temperature.

In the absence of an applied field we find that:

$$\langle S_z^1 \rangle = -\langle S_z^2 \rangle \qquad \text{A2}$$

implying that the average spin per atom is always zero. The Néel temperature is found by taking the small argument expansion of each equation and insisting that the determinant of the matrix of coefficients of the resulting linear equations equals 0. We find:

$$T_N = \frac{S(S+1)\, z|J|}{3k_B} \qquad \text{A3}$$

which is equivalent to Eq.(20) above.

## APPENDIX V A FURTHER EXAMPLE OF CONVERGENCE IN 1-D

The following figures illustrate the convergence of solutions for normalized average spin as a function of temeprature on going to higher order models. The parameters are $S^A = 0.5$, $S^B = 1.5$, $J_{AA} = 50\text{K}$, $J_{AB} = 65\text{K}$, $J_{BB} = 80\text{K}$, $z = 2$.

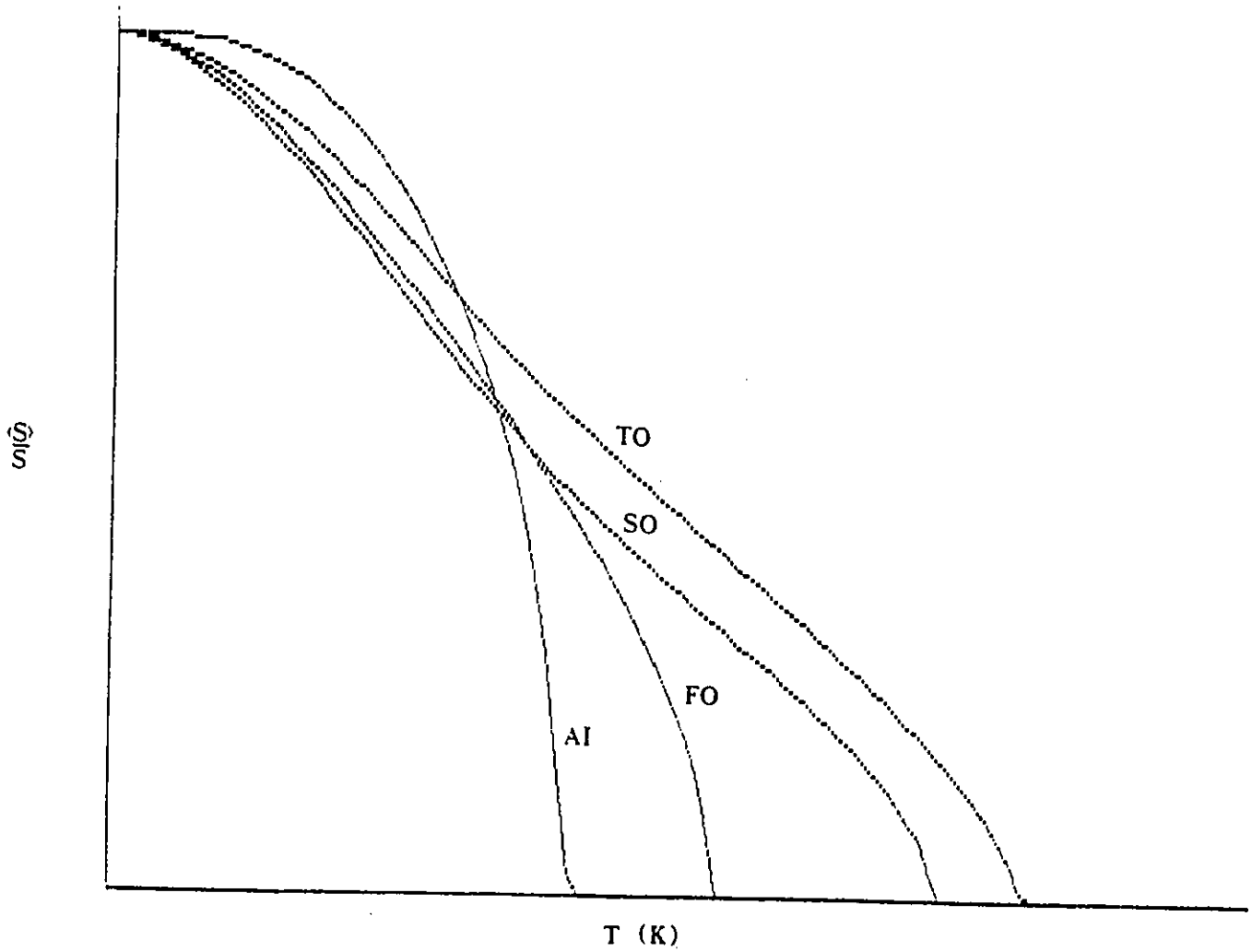


Fig. A3 Normalized average spin per atom vs. temp. as obtained by TO, SO, FO and AI models.

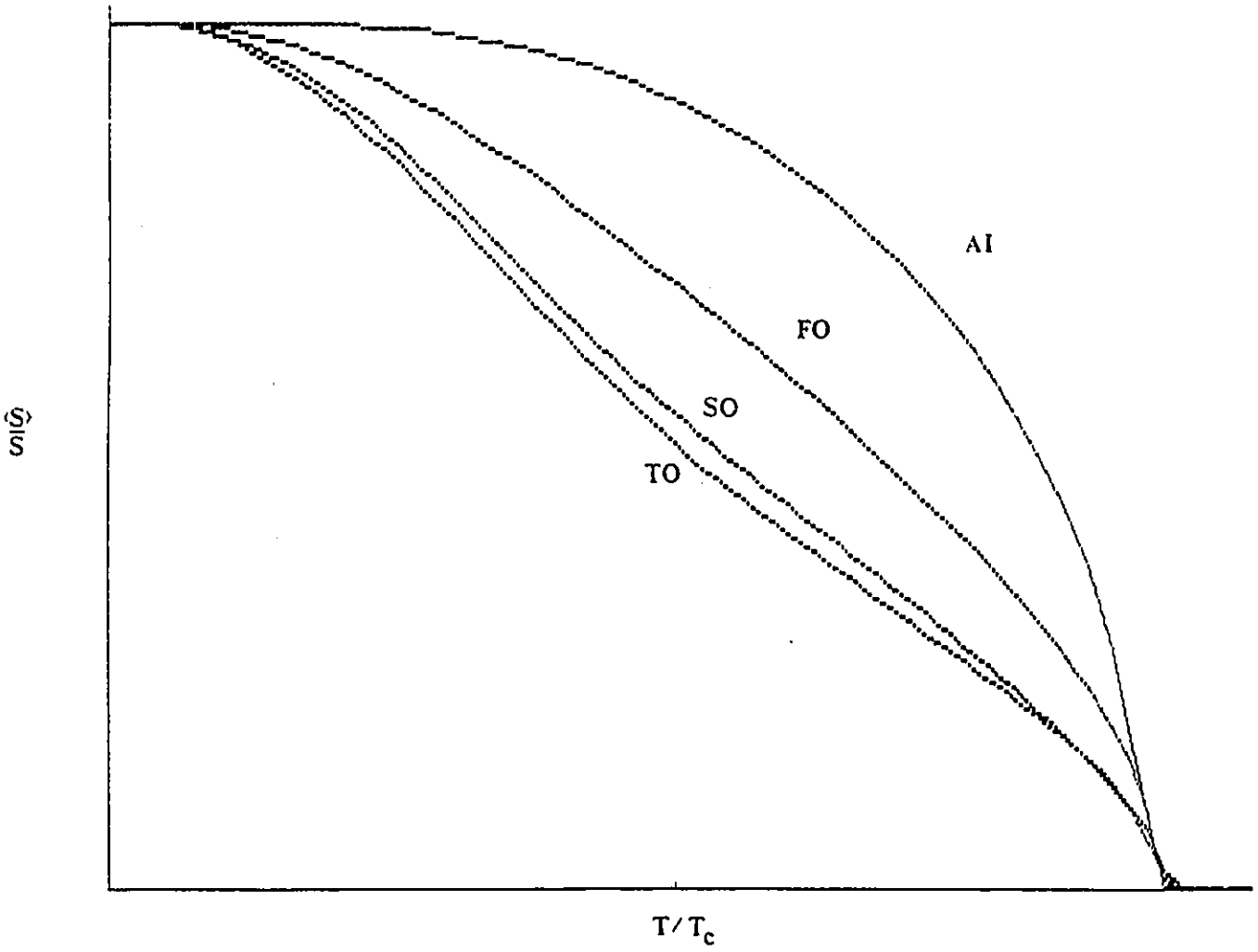


Fig. A2 Normalized average spin per atom vs. $T / T_C$ as obtained by TO, SO, FO and AI models.

## REFERENCES


1. Neil W. Ashcroft and N. David Mermin, Solid State Physics, Saunders College, (Philadelphia, PA, 1976)

2. J.S. Smart, Effective Field Theories of Magnetism, W.B. Saunders Co. (Philadelphia, PA, 1966)

3. D.G. Rancourt, "The Invar Problem" (Review), *Physics in Canada*, Jan. 1989, 3-10.

4. Sumiyoshi Fujiki, "Magnetovolume Effect in Site-Random FCC : Application to FeNi Alloy", *J. Magn. Mat.* **31-34** (1983), 101-102.

5. M. Fähnle, On the Temperature Dependence of the Spontaneous Magnetization in Amorphous Ferromagnets", *Solid State Commun.* **49** (1984), 391-394.

6. C.G. Montgomery, J.I. Krugler and R.M. Stubbs, "Green's-Function Theory of a Disordered Heisenberg Ferromagnet", *Phys. Rev. Lett.* **25** (1970), 669-672.

7. J.R. Thompson et al, "Monte Carlo Simulations of Transverse Spin Freezing in the Three-Dimensional Frustrated Heisenberg Model", *J. Appl. Phys.* **69** (1991), 5231-5233.

8. Marc Gabay and Gérard Toulouse, "Coexistence of Spin-Glass and Ferromagnetic Orderings", *Phys. Rev. Lett.* **47** (1981), 201-204.

9. T. Kaneyoshi, "Magnetic Properties of a Mixed Spin Ising Model with Random Nearest-Neighbour Interactions", *J. Magn. Mat.* **92** (1990), 59-67.

10. K. Handrich, "A Simple Model for Amorphous and Liquid Ferromagnets", *Phys. Stat. Sol.* **32** (1969), K55-K58.

11. S.K. Sidorov, A.V. Doroshenko and S.F. Dubinin, "Concentrational Dependence of the Magnetization of Some Transition-Metal Alloys", *Journal de Physique* **32** (1971) C1 870-C1 871.

12. J.B. Müller and J. Hesse, "A Model for Magnetic Abnormalies (sic) of FeNi Invar Alloys", *Z. Phys. B-Condensed Matter* **54** (1983), 35-42.

13. A.Z. Menshikov, "Invar Effect by Local Moment Model", *J. Magn. Magn. Mat.* **5** (1977), 188-195.

14. A.Z. Menshikov, "Local Moment Model for the Invar Effect", *J. Magn. Magn. Mat.* **10** (1979), 205-213.

15. E.Z. Valiev and A.Z. Menshikov, "Linear and Non-Linear Magnetoelastic Interactions in the Molecular Field Theory and Invar Anomalies", *J. Magn. Magn. Mat.* **46** (1984), 199-206.

16. J.Y. Ping, D.G. Rancourt and R.A. Dunlap, "Physical Basis and Break Down of Hyperfine Field Distribution Analysis in fcc Fe-Ni",in press, *J. Magn. Magn. Mat.*

17. J. Crangle and G.H. Hallan, "The Magnetization of face-centred cubic and body-centred cubic iron and nickel alloys", *Proc. Roy. Soc. A* **272** (1963). 119

18. D.G. Rancourt and J.Y. Ping, "Voigt-Based Methods for Arbitrary-Shape Static Hyperfine Parameter Distributions in Mössbauer Spectroscopy", *Nucl. Instr. Methods* **B58** (1991), 85-87.

19. J. Hesse and C.H.R. Buchal, "Mössbauer Measurements of Effective Exchange Fields at Fe-Impurities in Ni and $Ni_{80}Co_{20}$", *Int. J. Magn.* **5** (1973), 11-14.

20. D.G. Rancourt and J.Y. Ping, "Measured and Predicted Hyperfine Field Distributions (HFD's) in fcc Fe-Ni Collinear Ferromagnets", submitted to ICAME '90. To appear in *Hyp. Int.* (1992).